Chapter-IV

Results and Discussion

Chapter IV
Results and Discussion

4.1 Mechanochemically Synthesized Leucite for Dental Veneering Glass Ceramics

4.1.1 Phase analysis

Fig. 4.1 shows the XRD patterns of leucite samples heat treated at varying temperatures. It is noted from Fig. 4.1 that XRD pattern of the mixes fired at 900 °C for 1 h has kalsilite as a major phase with small peaks of the crystalline leucite. Furthermore, heat treatment was increased to 1000 °C, where leucite occurred as a major phase and peaks of meta-stable kalsilite diminished.

At 1100 °C, complete leucite phase formation occurred along with small amount of glassy phase. It is therefore, concluded that increasing the temperature plays a major role in the complete phase formation of crystalline leucite. It may be interpreted that metastable kalsilite reacted with residual vitreous SiO_2, converting into the crystalline leucite phase.

Therefore, these compositions were mixed with LTF in a weight ratio of 25:75 for further characterizations.

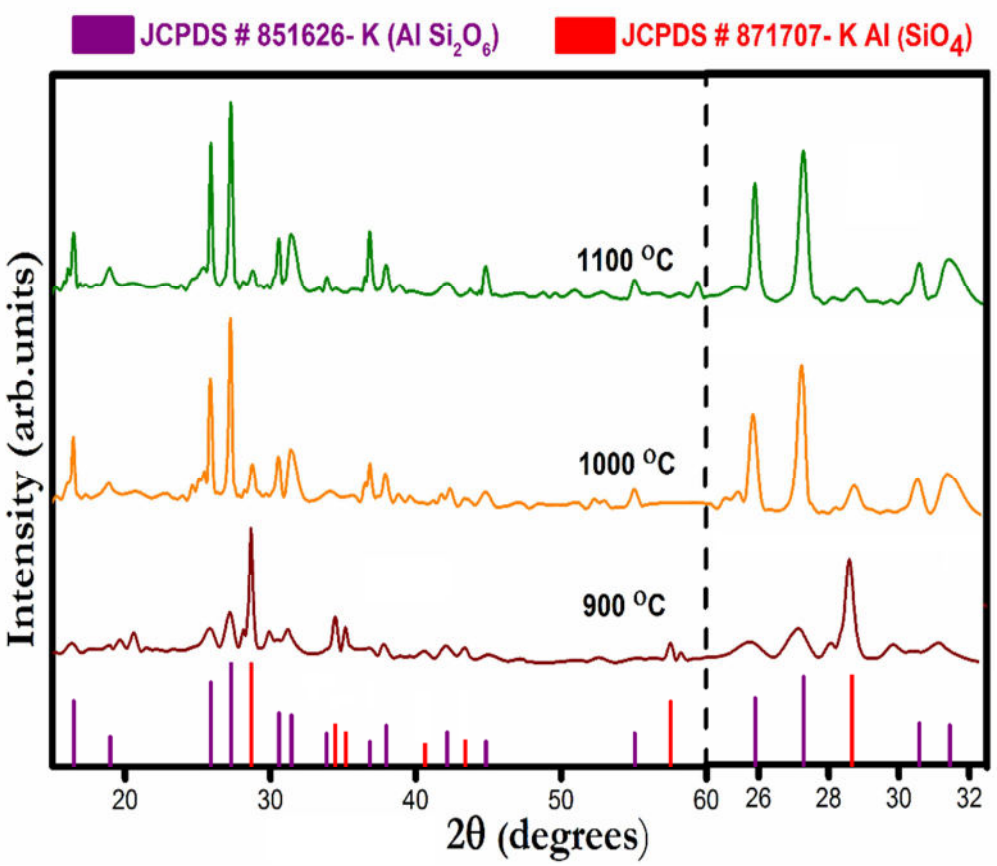

Fig. 4.1 X-ray diffraction patterns of 6 h milled leucite samples heat treated at different temperatures

The existence of broad peaks in the XRD pattern indicates the formation of nanocrystalline leucite. The above explanation is also supported by studies of Zhang et al. They reported that kalsilite phase disappears either at high temperatures or by increasing the soaking period [Zhang Y. (b) *et al.* 2007]. It is noted that compositions heat treated at 1000 and 1100 °C having high a concentration of leucite than that of the sample heated at 900 °C.

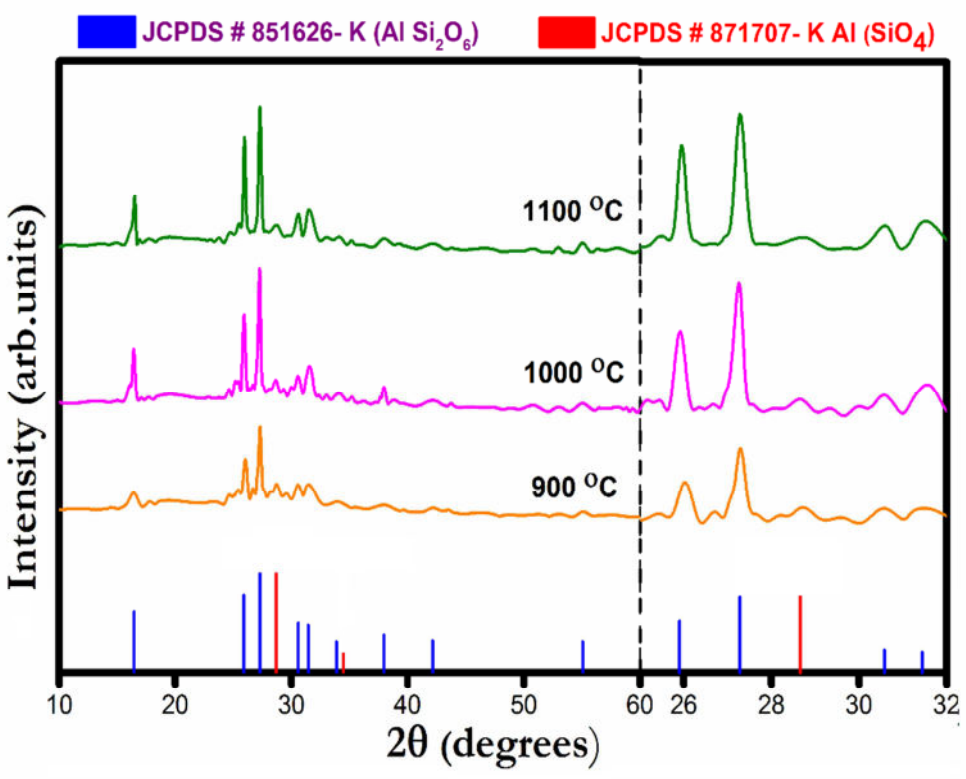

Fig. 4.2 X-ray diffraction patterns of leucite with 2 wt. % of CaF_2 heat treated at different temperatures

Fig. 4.2 shows the XRD patterns of 6 h milled leucite containing 2 wt. % of CaF_2 and heat treated at 900, 1000 and 1100°C for 1 h. Leucite crystalline phase is formed in all the samples with a very small amount of kalsilite crystalline phase at 900 °C. No secondary crystalline phase is identified in the samples fired at 1000 and 1100 °C. It is anticipated that presence of CaF_2 additive suppressed the crystallization of kalsilite and it has also been reported earlier [Zhang Y. *et al.* 2006]. A small amount of CaF_2 (2 wt. %) is therefore, essential for good crystallization of tetragonal leucite.

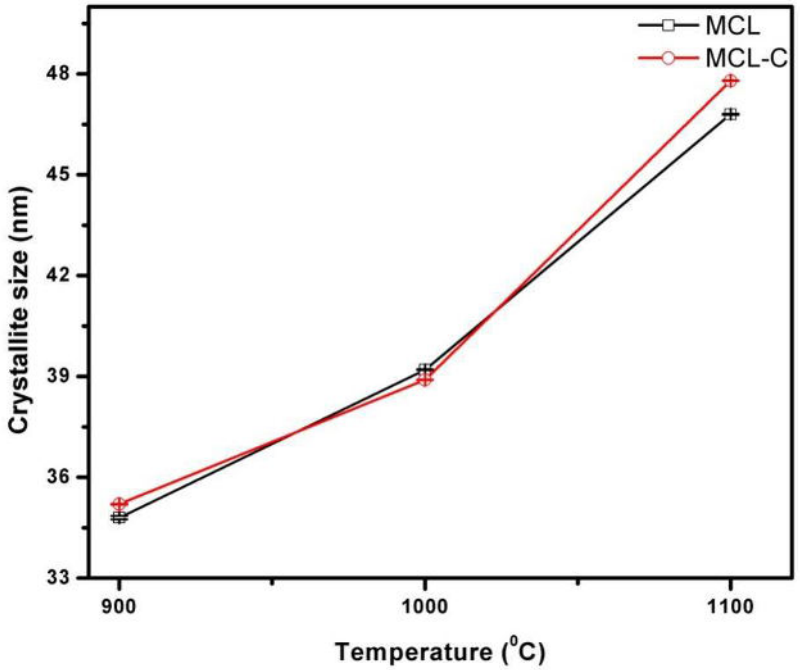

Fig. 4.3 Variation of crystallite size of the leucite samples with & without CaF_2 with temperature

Leucite phase formation at 900°C indicates that CaF_2 lowers the synthesis temperature of leucite and suppress the formation of kalsilite meta-stable phase as well as the amorphous phase. The nanocrystalline powder is formed as a result of high energy ball milling. Fig. 4.3 demonstrates the crystallite size of the samples as a function of temperature. From this plot, it is observed that crystallite size increases with the temperature. This is because of grain growth at higher temperatures.

4.1.2 Coefficient of thermal expansion (CTE)

CTE is the most significant characteristic for reliable PFM restoration. Thermal compatibility of the ceramics fused to metal from room temperature to the glass transition temperature can be assessed by matching the average expansion coefficient of the metal and porcelain in the temperature range 20-550 °C. Fig. 4.4 illustrates the CTE curves of the compositions, LTF, MCL_{1000}, MCL_{1100}, MCL-C_{1000} and MCL-C_{1100}. The glass transition temperatures (T_g) of the LTF, MCL_{1000}, MCL_{1100}, MCL-C_{1000}, and MCL-C_{1100} were determined to be 395, 405, 415, 425 and 430 °C respectively.

Table 4.1 CTE, glass transition temperature (T_g) and softening point (SP) of all the samples fired at different temperature

Sample Coding	CTE (/°C)	Tg (°C)	SP (°C)
MCL_{1000}	10.1×10^{-6}	405	475
MCL_{1100}	14.2×10^{-6}	415	480
MCL-C_{1000}	15.3×10^{-6}	425	485
MCL-C_{1100}	15.7×10^{-6}	430	495

CTE of the samples before T_g is found to be 10.1×10^{-6}/°C, 14.2×10^{-6}/°C, 15.3×10^{-6}/°C and 15.7×10^{-6}/°C for the compositions, MCL_{1000}, MCL_{1100}, MCL-C_{1000} and MCL-C_{1100} respectively. It is due to high crystalinity of leucite phase (as seen by XRD results also) at 1100 °C than that at 1000 °C leads to high CTE. However, in the case of MCL-C_{1000} and MCL-C_{1100}, CaF_2 stabilizes the leucite phase even at 1000 °C and therefore there is not much difference between the CTE at 1000 and 1100 °C.

Values of CTE of all the compositions are given in Table 4.1. These prepared materials are suitable for PFM as its CTE value is close to the standard CTE of (14.5 × 10^{-6}/°C) of dentine Vita VMK 95 Dentine 1M2. It is concluded that addition of leucite to LTF matrix enhances the CTE of the whole mixture. This is due to the homogeneous distribution of fine leucite particles throughout the matrix.

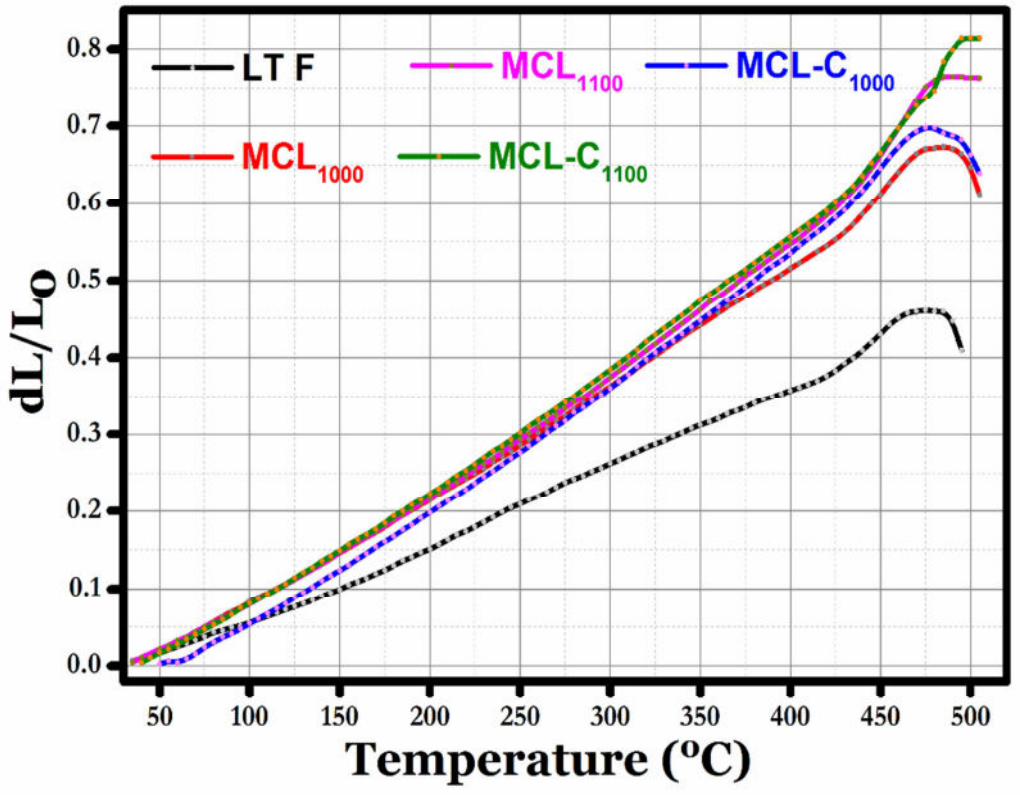

Fig. 4.4 CTE curves of the compositions, LTF, MCL_{1000}, MCL_{1100}, $MCL\text{-}C_{1000}$ and $MCL\text{-}C_{1100}$

4.1.3 Microstructure

The surface morphology of the compositions, MCL_{1100} and $MCL\text{-}C_{1100}$ at different magnifications is shown in Fig. 4.5. The images show the homogenous distribution of tetragonal leucite crystals throughout the matrix. There is no visible micro-crack due to phase transformation of meta-stable kalsilite to leucite.

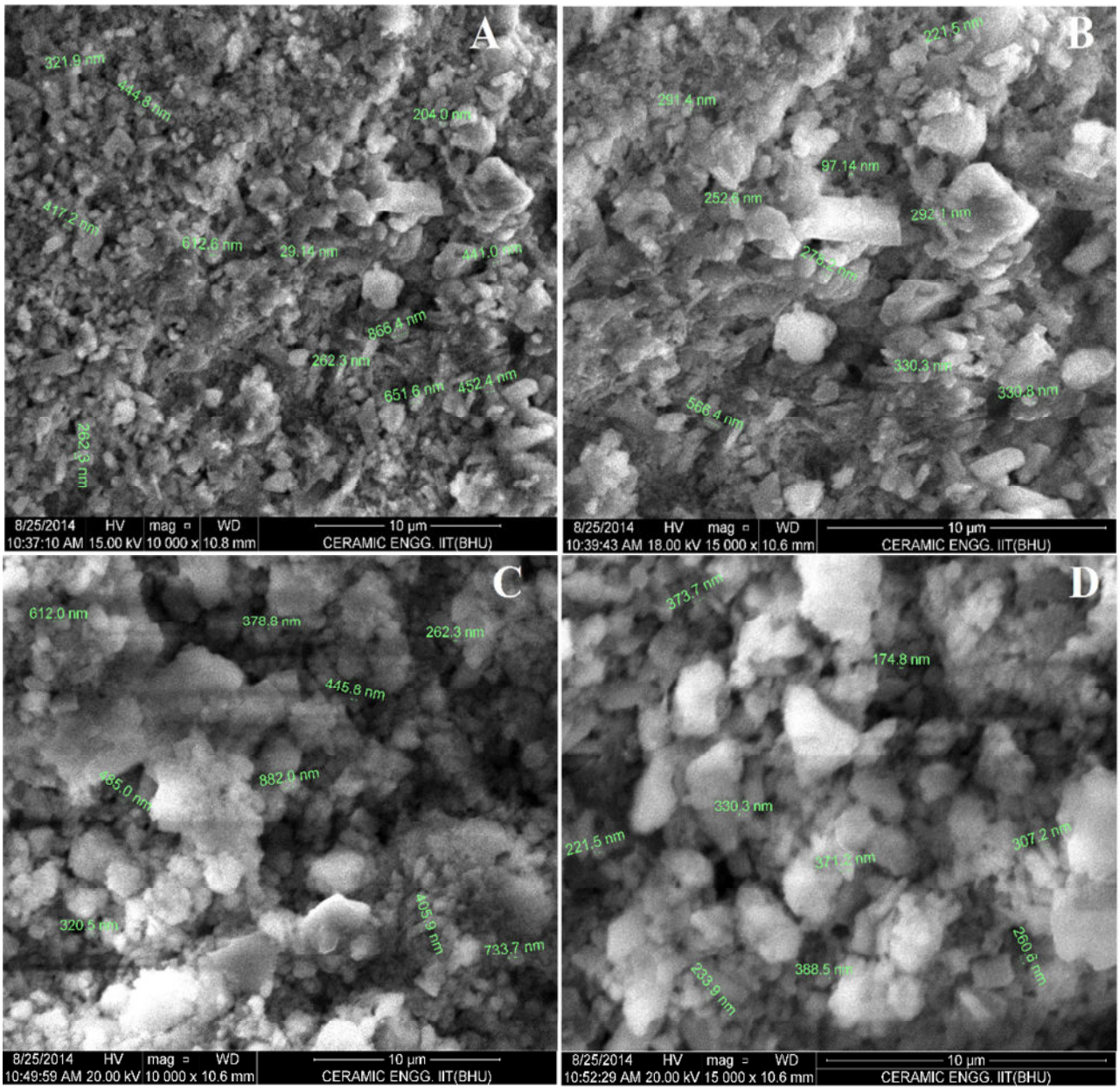

Fig. 4.5 SEM micrographs of samples fired at 800 ºC at different magnifications (A, B) MCL_{1100} and (C, D) MCL-C_{1100}

The average grain size of the leucite crystal determined from ImageJ software is in the range 0.6 to 1.0 μm. Some previous studies suggest that fine leucite crystal is beneficial for the enhancement of mechanical property [Chen X. *et al.* 2011]. Fine grain leucite also increases the abrasion resistance [Holland W. *et al.* 2009].

4.1.4 Flexural strength

Fig. 4.6 shows the flexural strength of MCL and MCL-C samples as a function of the temperature. Flexural strength of the sample MCL-C is slightly higher than that of MCL. The homogenous dispersion of leucite grains within the glassy matrix leads to its enhanced mechanical strength [Sheu T.S. *et al.* 1994]. Moreover, the synthesized nanocrystalline leucite powders have large surface area. Subsequently, the samples produced show better sinterability, low porosity, and high flexural strength. MCL and MCL-C samples heat treated at 900 °C show less flexural strength among the series.

This is correlated with the presence of meta-stable kalsilite phase at 900 °C which has low flexural strength than the leucite. The samples MCL_{1100} and MCL-C_{1100} show highest flexural strength than the rest of the batch. The less significant difference has been observed between the samples MCL_{1000}-MCL-C_{1000} and MCL_{1100}-MCL-C_{1100} as compared to samples MCL_{900}-MCL-C_{900}. In other words, leucite materials have better flexural strength than the glass materials. This is the reason that incorporation of CaF_2 in the composite increases the flexural strength because of more formation of leucite.

Table 4.2 Flexural strength and Weibull statistical parameters of all the samples

Sample Coding	Mean (MPa)	SD (MPa)	m	σ_0 (MPa)	r^2
MCL_{1000}	41.28	1.580	25.00	42.52	0.974
MCL_{1100}	43.49	1.210	33.67	44.25	0.980
$MCL\text{-}C_{1000}$	44.00	1.000	28.68	45.15	0.973
$MCL\text{-}C_{1100}$	46.87	1.036	38.08	46.99	0.966

*SD-Standard Deviation; m-Weibull modulus; σ_0-Characteristic strength;

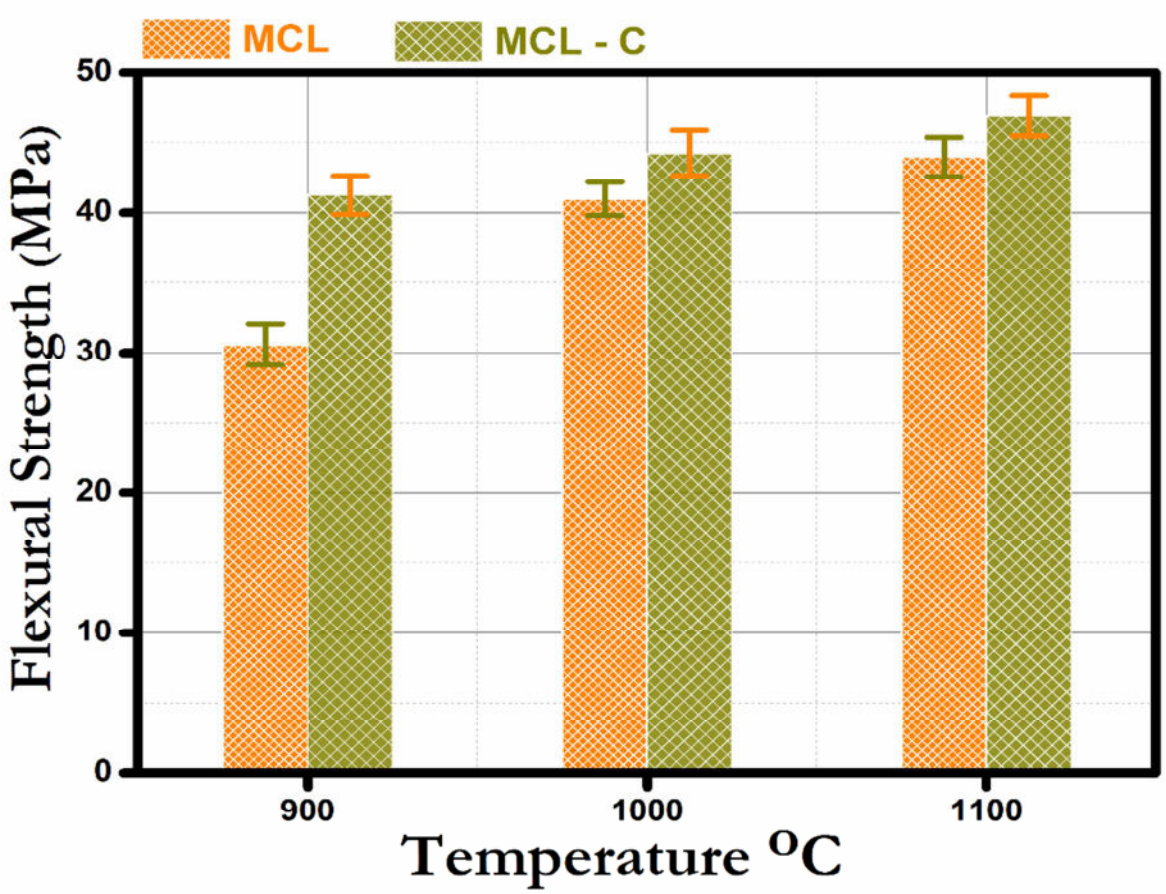

Fig. 4.6 Flexural strength of MCL and MCL-C samples heated at different temperatures

This is due to less concentration of leucite crystalline phase present in MCL_{900} as compared to MCL-C_{900} (as seen by XRD Figs. 4.1 & 4.2). In the case of samples MCL_{1000}-MCL-C_{1000} and MCL_{1100}-MCL-C_{1100}, however, the leucite is present as a major phase (Figs. 4.1 & 4.2) and therefore, shows a less significant difference in the flexural strength. It is, therefore, inferred that addition of CaF_2 improves the flexural strength. As the ionic radius of F^- ion (1.33 Å) is similar to the O^{2-} ion (1.40 Å) and hence replace the O^{2-} ion easily and form either Si-O or Al-O bond, it is also reported earlier [Zhang Y. *et. al* 2006]. This consequently loses the glassy network. Meanwhile, Ca^{2+} ion attracts with O^{2-} ion and can form eutectoid in the system and lower the potential for the phase transformation [Y. Zhang *et. al* 2006]. This can help in the transformation of amorphous phase to ordered structure and crystallizes the leucite phase at a lower temperature. The crystalline phase has high flexural strength as compared to amorphous phase. Thus, the addition of CaF_2 crystallizes the leucite phase and suppresses the amorphous phase and hence improves the flexural strength. The mean and standard deviation values and Weibull statistical parameters of the strength data are given in Table. 4.2. It is noted from Table. 4.2 that values of Weibull modulus and nominal strength of the MCL-C samples are higher than that of the MCL samples. A high value of Weibull modulus confirms the reliability of these samples [Klein C.A. *et al.* 2004].

4.1.5 Ion leachability and surface morphology

Fig.4.7 shows weight loss of the MCL and MCL-C samples after immersion in 4% acetic acid and pineapple juice. It is noted from Fig. 4.7 that weight loss of all the leucite samples is less in the acetic acid than that in the pineapple juice.

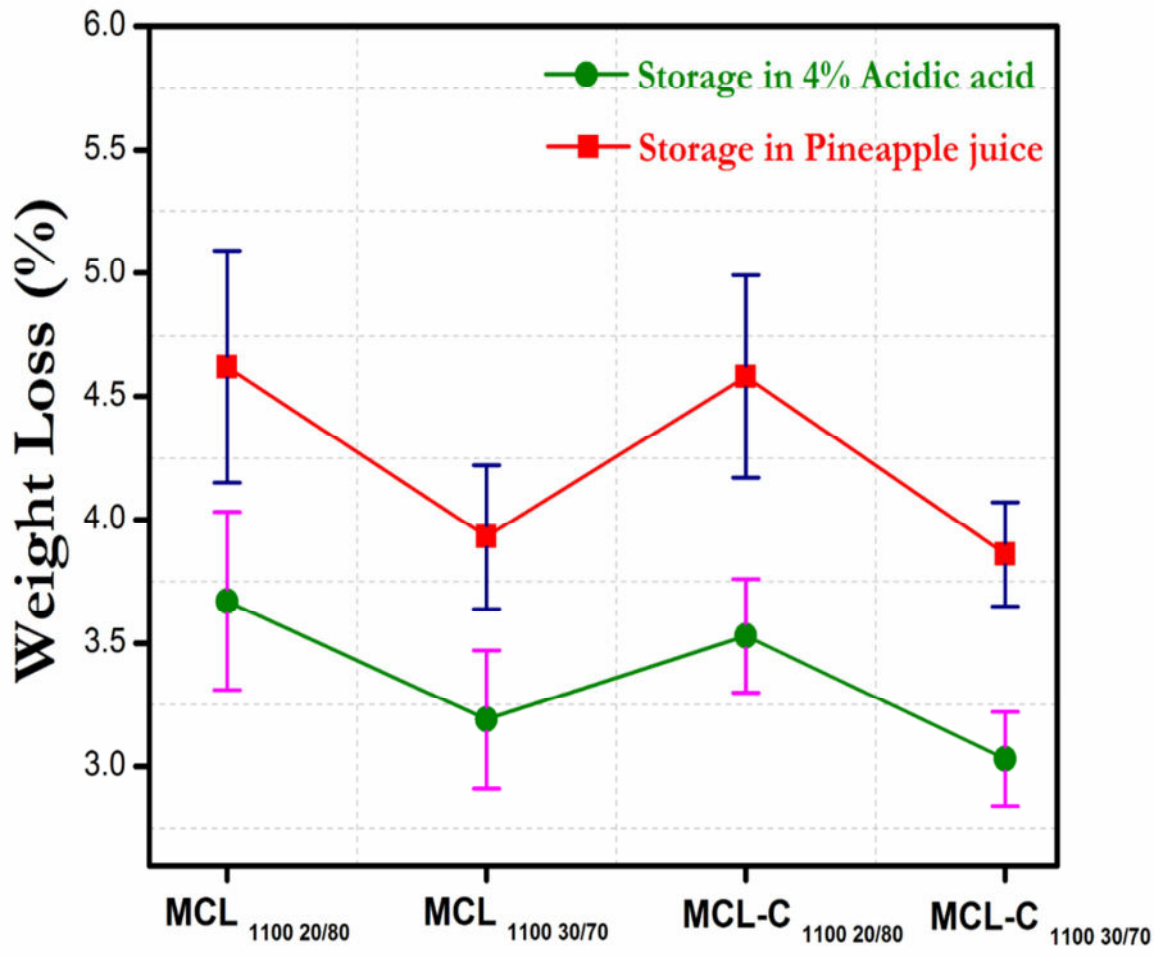

Fig. 4.7 Weight loss of the MCL and MCL-C samples after immersion in 4% acetic acid and pineapple juice

Weight loss decreases with increasing the content of the nanocrystalline leucite in the LTF matrix. This is due to the homogeneous distribution of leucite throughout the matrix. There is a very less significant difference between the samples MCL and MCL-C samples. The amounts of leached elements from the surface of leucite glass ceramic have been evaluated and are reported in Table. 4.3. The leaching of K^+ and Ca^+ in $MCL_{20/80}$ samples is higher. In these samples leucite phase ($K_2O.Al_2O_3.2SiO_2$) is lower. Therefore, some K^+ and Ca^+ ions can be in free state not dissolved in glass. The unreacted K+ and Ca+ ion can be easily leached out. In 4% acetic acid and pineapple juice, the highest leaching values of sodium and potassium ions have been observed in $MCL_{20/80}$ and MCL-$C_{20/80}$ samples (Table.4.3). Furthermore, in both 4% acetic acid and pineapple juice, the lowest leaching values of sodium and potassium have been found in $MCL_{30/70}$ and MCL-$C_{30/70}$ samples (Table.4.3).

Fig. 4.8 shows the surface morphology of the leucite samples before immersion in the acidic agents. It is seen that surface is very dense and glossy. Fig. 4.9 shows the surface morphology of the samples after immersion in 4% acetic acid for 168 hrs. at 80 ºC.

It is seen from Fig. 4.9 that after immersion for 168 hours in 4% acidic agent, the surface becomes rough and some open porosity portions have also been observed with reduced glassy surface. The maximum roughness and surface defects have been observed in the MCL samples.

Table. 4.3 Leaching of ions from the leucite samples after immersion in 4% acetic acid and pineapple juice for 168 hrs.

Leaching of ions from sample after immersion in storage agents for 0 and 168 hours	Storage agent	Time (hour)	Mean Ion leaching (µg/cm^2) (SD)		
			Na	K	Ca
$MCL_{20/80}$	4% Acetic acid	0	105 (8.1)	5 (0.3)	255 (13.6)
		168	298.92 (12.21)	284.45 (11.60)	201.22 (13.88)
	Pineapple juice	0	185 (28)	5250.22 (102)	448 (16.5)
		168	310.64 (22.80)	5830.66 (211.90)	1865.88 (86.14)
$MCL_{30/70}$	4% Acetic acid	0	105 (8.1)	5 (0.3)	255 (13.6)
		168	264.48 (57.3)	206.46 (10.66)	176.22 (9.62)
	Pineapple juice	0	185 (28)	5250 (102)	448 (16.5)
		168	314.16 (17.924)	5656.18 (196.44)	1682.20 (72.50)
MCL-$C_{20/80}$	4% Acetic acid	0	105 (8.1)	5 (0.3)	255 (13.6)
		168	214.84 (19.51)	182.42 (11.16)	148.10 (8.96)
	Pineapple juice	0	185 (28)	5250 (102)	448 (16.5)
		168	294.74 (16.71)	5745.84 (169.62)	1546.08 (70.30)
MCL-$C_{30/70}$	4% Acetic acid	0	105 (8.1)	5 (0.3)	255 (13.6)
		168	214.76 (18.17)	161.45 (15.95)	123.60 (8.32)
	Pineapple juice	0	185 (28)	5250 (102)	448 (16.5)
		168	260.58 (52.42)	5441.58 (161.25)	1392.80 (68.62)

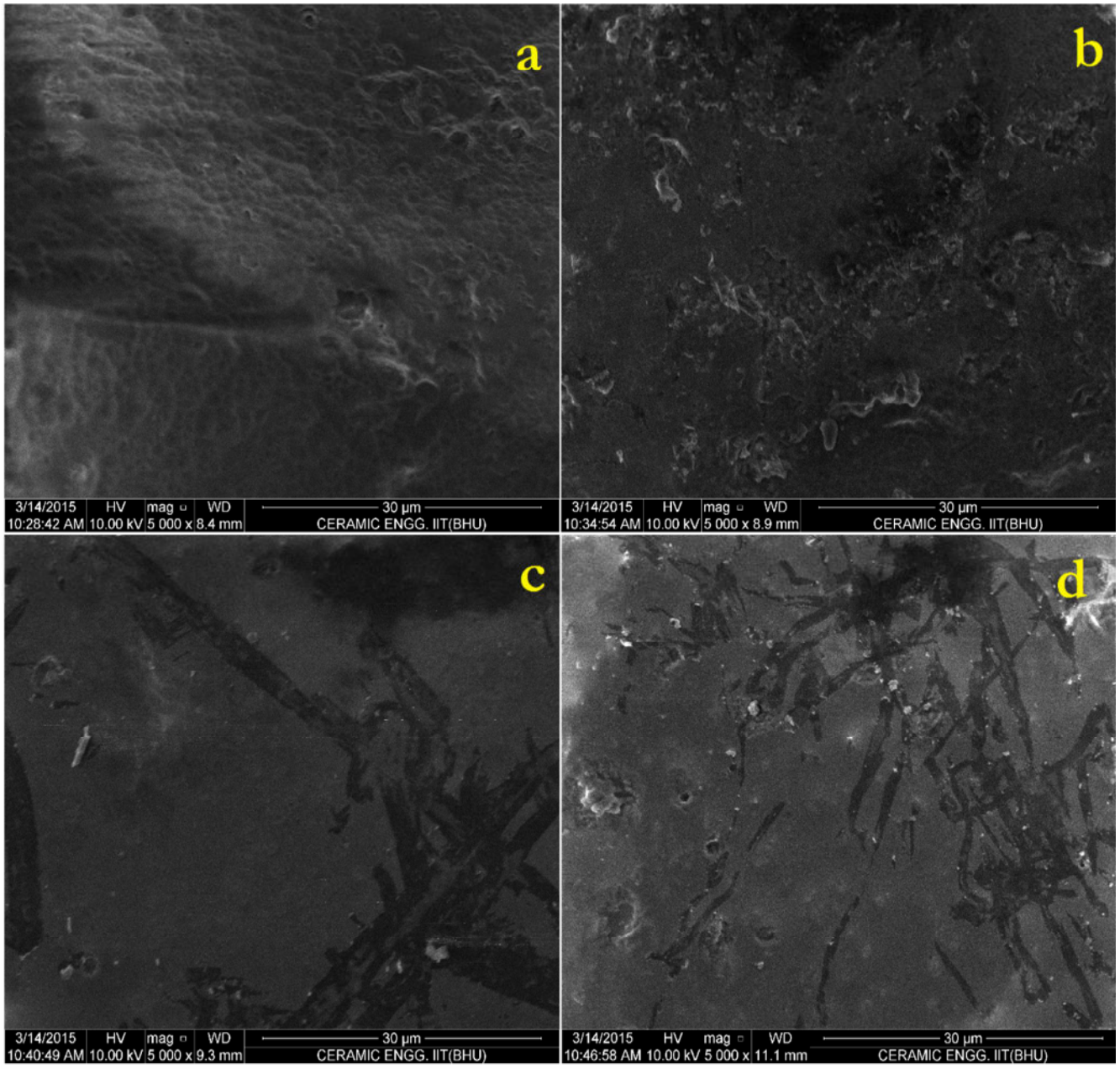

Fig. 4.8 SEM micrograph of the leucite samples before immersion in acidic medium a) $MCL_{20/80}$; b) $MCL_{30/70}$; c) MCL-$C_{20/80}$and d) MCL-$C_{30/70}$

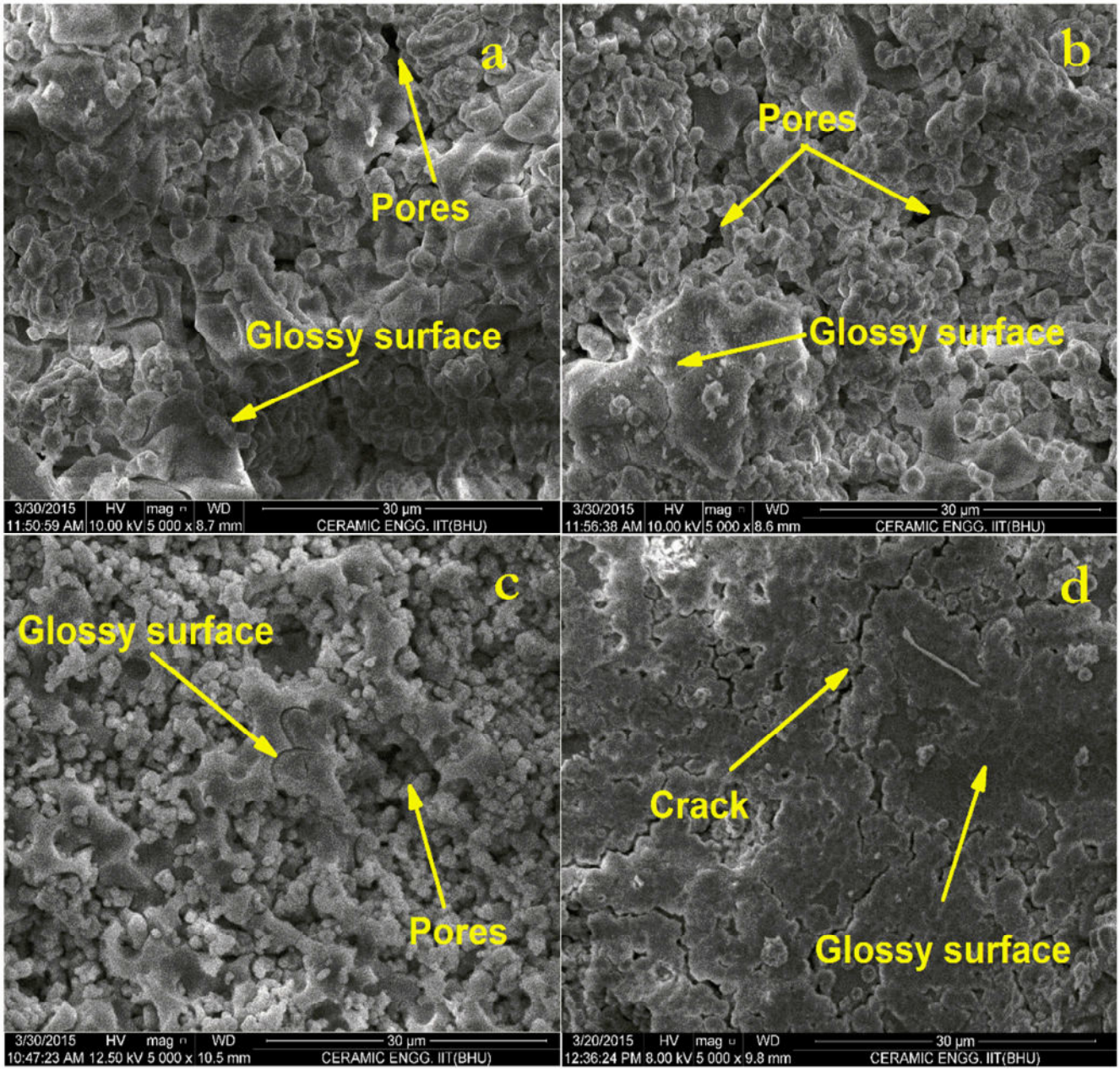

Fig. 4.9 SEM micrograph of the leucite samples after immersion in 4% acetic acid for 168 hours at 80°C, medium a) $MCL_{20/80}$; b) $MCL_{30/70}$; c) MCL-$C_{20/80}$ and d) MCL-$C_{30/70}$

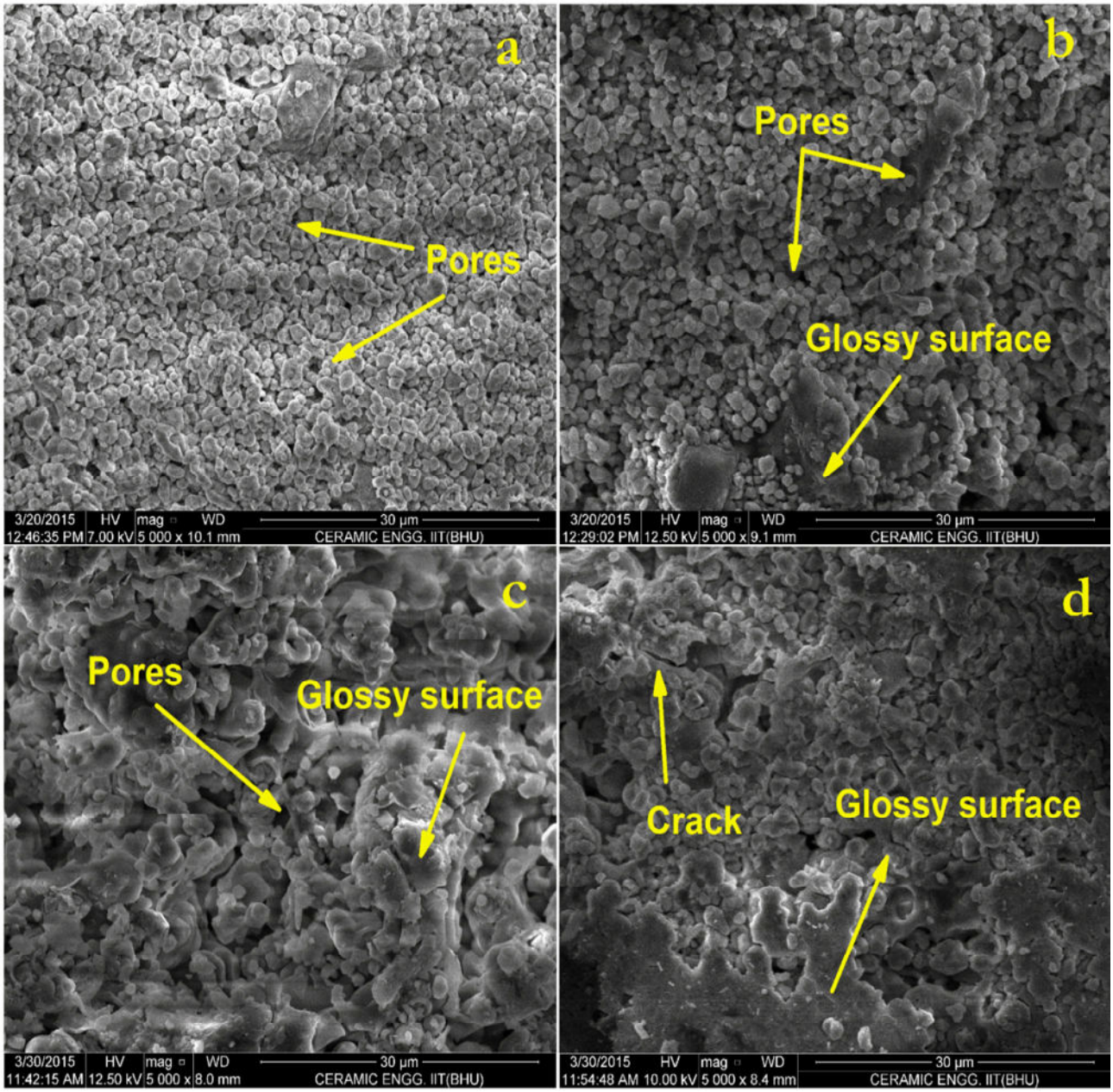

Fig. 4.10 SEM micrograph of the leucite samples after immersion in pineapple juice for 168 hours, a) $MCL_{20/80}$; b) $MCL_{30/70}$; c) MCL-$C_{20/80}$ and d) MCL-$C_{30/70}$

Composition, MCL-$C_{30/70}$ has the minimum roughness and this is also in conformity with the weight loss results. It is also seen that the porosity and surface roughness decreases with increasing the leucite content in the LTF. Fig. 4.10 shows the surface morphology of the leucite samples after immersion in pineapple juice for 168 hrs at 80 ºC. It is noted from Fig.4.10 that roughness and porosity at the surface of all the leucite samples are high as compared to that of Fig. 4.9. This is also in conformity with the Fig. 4.7 that weight loss in pineapple juice is greater than that in the 45 acetic acid.

4.1.6 Summary of the results

Leucite glass-ceramic has been successfully synthesized using mechanochemical synthesis route relatively at low temperatures after the introduction of 2 wt. % of CaF_2 as an additive. The introduction of CaF_2 in leucite raw mixes suppressed the formation of kalsilite phase. The Coefficient of thermal expansion of the samples with the mixes of leucite nanocrystalline powders and low-temperature frit nearly matched with the coping material (nickel-chrome alloy). The veneering dental glass–ceramics prepared by using these materials may be used in various applications for making PFM crowns or bridges. The composition of these mixes can be adjusted to obtain a different value of thermal expansion by varying prepared leucite content. In this new approach, glass-ceramic powders for opaque, dentine and glazes for veneering applications can be prepared which have different melting temperatures and thermal expansion value. It is also noted that values of Weibull modulus increase with increasing the temperature. This may be due to increase in the content of fine leucite crystals. These higher values confirm the reliability of these samples which is beneficial for its mechanical properties. MCL samples have high ion leachability

than that of the MCL-C samples. Compositions MCL_{1100} and $MCL\text{-}C_{1100}$ show the better properties among the series, therefore, it has been chosen for the bioactive glass ceramic composites.

4.2 Mechanochemical Synthesis of Kalsilite: Implementation as Dental Porcelain with Low Temperature Frit

4.2.1 Phase analysis

Fig. 4.11 shows the XRD patterns of the kalsilite samples milled for 3 h and heat treated at different temperatures. It is noted that XRD patterns of precursor heat treated at 900 and 1000 °C contains kalsilite as a major phase having a hexagonal crystal structure. Diffraction peaks are well matched to JCPDS card No. 87-1707. No second phase formation has been detected. The unit cell parameters are a = b = 5.157 and c = 8.706 Å and more similar to those reported by Becerro et al. [a = 5.166 and c = 8.7123 Å] [Becerro A.I. *et al.* 2009].

The presence of broad peaks in the XRD patterns confirms the formation of nanocrystalline kalsilite. Kalsilite samples milled for 3 h and heated at 900, 1000 and 1100 ºC have a crystallite size in the range 35-55 nm (determined using Scherrer's formula). Furthermore, heat treatment has increased to 1100 °C; kalsilite occurs as a major phase with some peaks of leucite crystalline phase. It is also noted that formation of leucite crystalline phase occurs at high temperature.

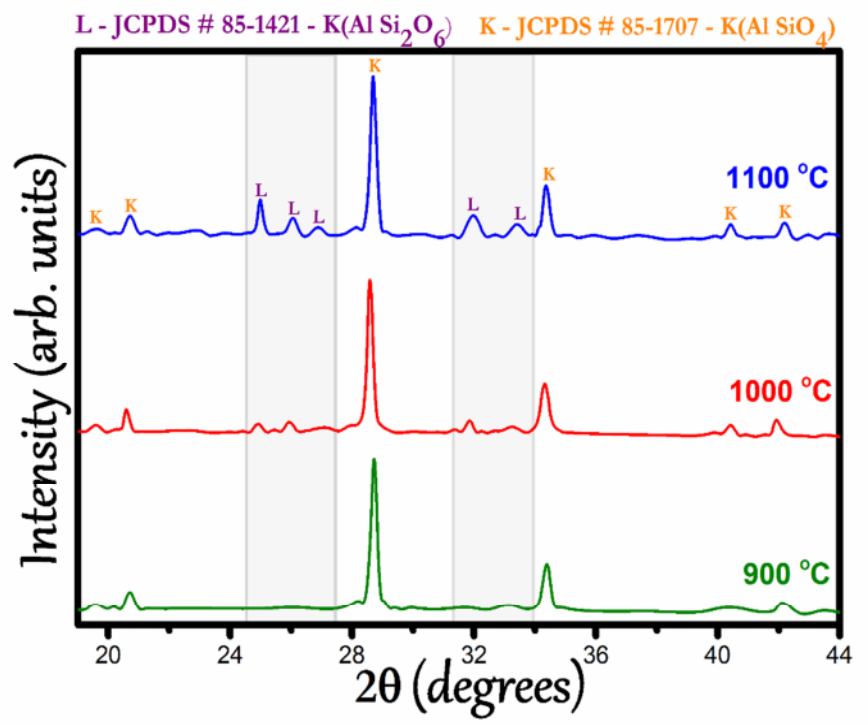

Fig. 4.11 XRD patterns of the kalsilite samples milled for 3h and heat treated at different temperatures

Fig. 4.12 shows the XRD patterns of the MgF_2 added kalsilite samples milled for 3h. It is seen that XRD pattern of the precursor heat treated at 900 and 1000 °C contains hexagonal kalsilite as a major phase alike to JCPDS card No. 87-1707. MgF_2 added kalsilite samples milled for 3 h and heated at 900, 1000 and 1100 ºC have a crystallite size in the range 36-57 nm.

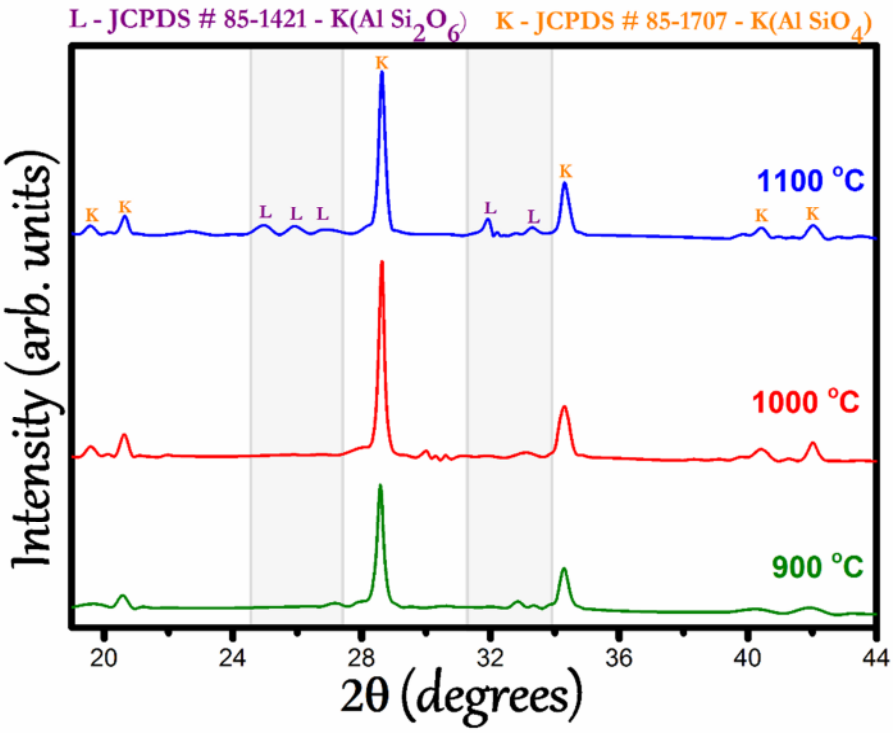

Fig. 4.12 XRD patterns of kalsilite with 2 wt. % of MgF_2samples milled for 3h and heat treated at different temperatures

As temperature increases from 1000 to 1100 °C kalsilite present as a major phase in addition to the small amount of leucite phase. Formation of leucite phase is less in the samples containing MgF_2 as compared to sample without MgF_2. It is probable that MgF_2 suppresses the crystallization of leucite phase.

Fig. 4.13 shows the XRD patterns of the kalsilite samples milled for 6 h. X-ray lines of sample heat treated at 900 °C contain kalsilite as a major phase with small peaks of leucite phase. At temperatures 1000 and 1100 °C, leucite presents as a major phase with small peaks of kalsilite crystalline phase. Kalsilite disappears after being extended heat treatment above 1100 °C. It happens due to high surface area of the ground samples.

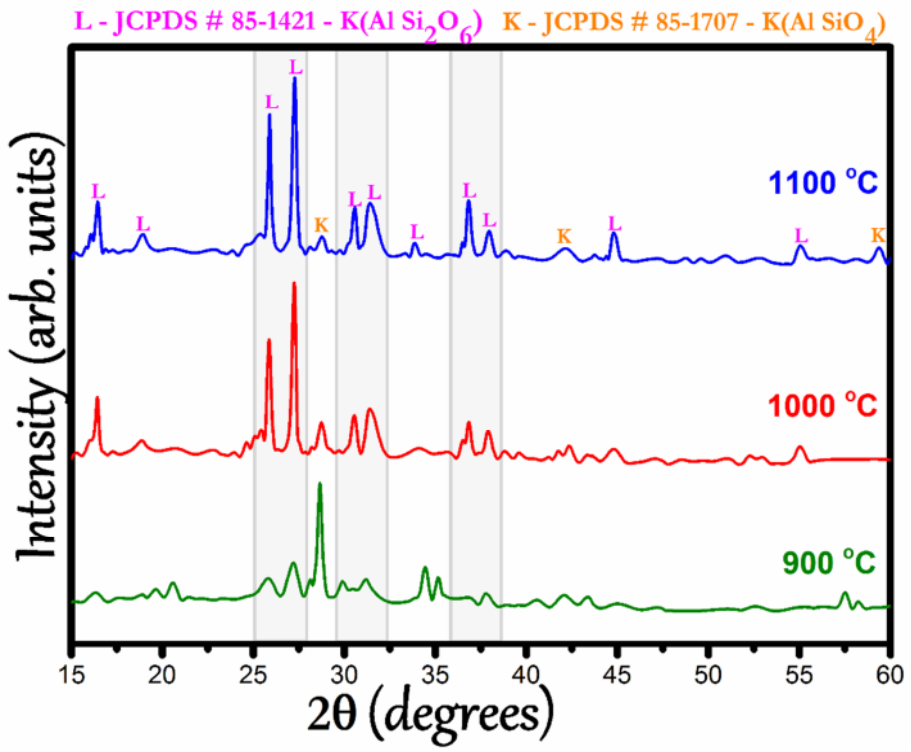

Fig. 4.13 XRD patterns of kalsilite samples milled for 6 h and heat treated at different temperatures

Kalsilite samples milled for 6 h and heated at 900, 1000 and 1100 ºC have a crystallite size in the range 25-35 nm. Smaller the particle size larger will be the surface area and hence the higher surface energy. It has also been previously reported that activation energy of formation of the leucite is superior to that of the kalsilite [Zhang Y. (a) *et al.* 2007].

Kalsilite, therefore, crystallizes first as a meta-stable phase and then reacts with residual SiO_2 which leads to the formation of leucite phase. In the present work, sample milled for 6 h has very fine particles as compared to the sample milled for 3 h. In the former case therefore, kalsilite converts into major leucite crystalline phase at the higher temperatures. This is due to the fact that surface energy of the fine particles is much greater as required for crystallization of the leucite phase.

Fig. 4.14 shows the XRD patterns of kalsilite samples containing 2 wt. % of MgF_2 milled for 6h and heat treated at different temperatures.

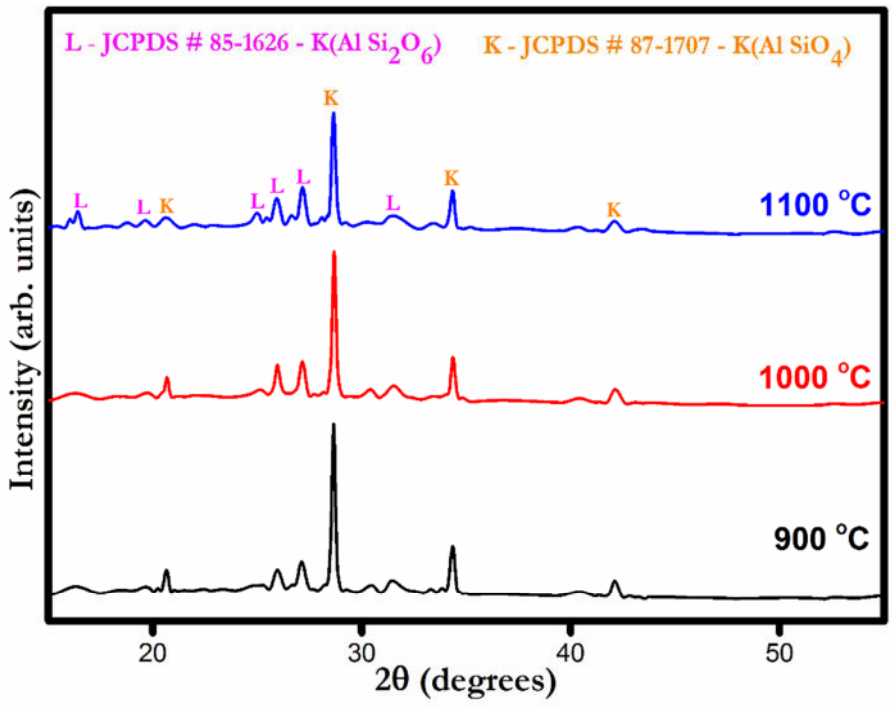

Fig. 4.14 XRD patterns of kalsilite with MgF_2 samples milled for 6 h and heat treated at different temperatures

It shows the presence of hexagonal kalsilite as a major phase with small peaks of leucite at 900, 1000 and 1100 °C. Diffraction peaks are well matched to JCPDS card No. 87-1707 and 85-1626. MgF_2 added kalsilite samples milled for 6 h and heated at 900, 1000 and 1100 ºC have a crystallite size in the range 28-37 nm.

Zhang et al. also studied the effect of the addition of CaF_2 on crystallization of leucite [Zhang Y. *et al.* 2006]. They observed that CaF_2 decreases the crystallization temperature of leucite. The Ionic radius of F^- ion (1.33 Å) is very close to the ionic radius of O^{2-} ion (1.40 Å), therefore it replaces the O^{2-} ion and forms the Si-F or Al-F bonds [Zhang Y. *et al.* 2006]. This consequently loses the glassy network. Meanwhile, Ca^{2+} ion attracts with O^{2-}

ion and can form eutectoid in the system and lower the potential for the phase transformation. This can help in the transformation of amorphous phase to ordered structure and crystallizes the leucite phase at a lower temperature. In the present work, whereas, MgF_2 inhibits the formation of leucite phase and stabilizes the kalsilite meta-stable phase. It is due to small amount of free silica present in the matrix. It is supposed that F^- ions replace the oxygen ions consequently loses the network so that Mg^{2+} ion react with free silica forms low-temperature eutectic phase such as enstatite (MgO. SiO_2). It will decrease the free silica content around the kalsilite in the matrix and suppress the formation of leucite. It is also noted that the kalsilite samples with & without MgF_2 and heat treated at 1000 ºC show better phase formation. Therefore, these samples have been mixed with LTF in different weight ratios for further characterizations.

4.2.2 Coefficient of thermal expansion (CTE)

Fig. 4.15 shows the CTE curves of the MKL samples. It is found that the increases in content of kalsilite in LTF containing glass ceramics increase the CTE of the whole matrix. Here secondary phase present as leucite in kalsilite glass-ceramics is also increasing. Therefore, higher CTE value is obtained in $MKL_{30/70}$ samples. Glass transition temperatures (T_g) of the samples, $MKL_{20/80}$, $MKL_{25/75}$ and $MKL_{30/70}$, are determined to be 415, 425 and 440 °C respectively. Fig. 4.16 shows the CTE curves of kalsilite with 2 wt. % of MgF_2 having different wt. % of LTF, MKL-$M_{20/80}$, MKL-$M_{25/75}$ and MKL-$M_{30/70}$.

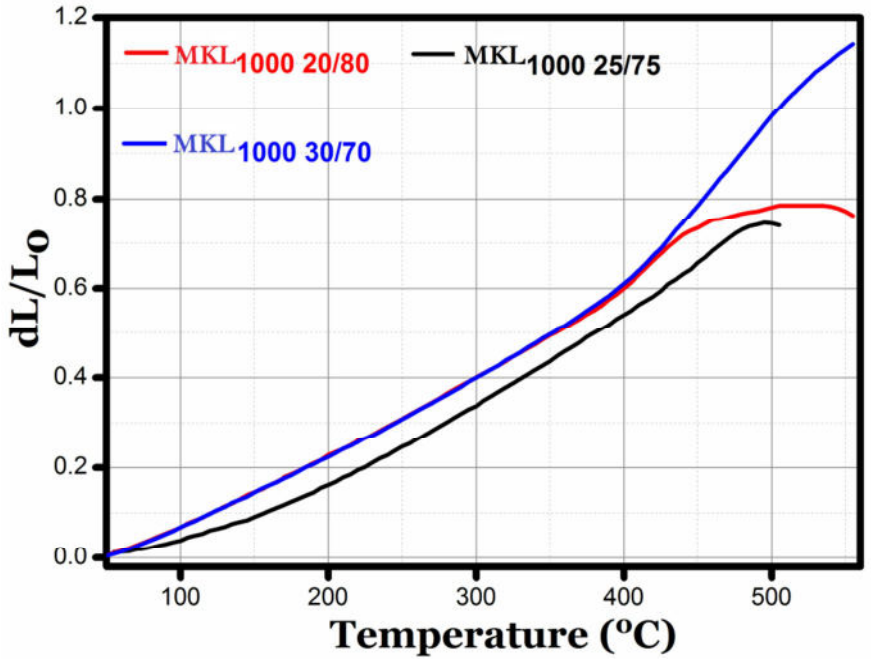

Fig. 4.15 CTE curves of the MKL samples containing different wt. % of kalsilite and LTF

It is observed that the addition of MgF_2 to kalsilite decreases the CTE of the final mixture. These CTE values are about 40% less than that of the samples without MgF_2. This is due to the formation of major kalsilite phase (as seen in Fig. 4.14) of low CTE. These results are in conformity with the results of XRD where samples containing MgF_2 has kalsilite as a major phase i.e. MgF_2 suppresses the formation of leucite. The glass transition temperatures (Tg) of the samples, MKL-$M_{20/80}$, MKL-$M_{25/75}$ and MKL-$M_{30/70}$ were determined to be 415, 425 and 430 °C respectively. All the MKL and MKL-M samples are suitable for PFM as its CTE value are in the range 14.0 to 14.8×10^{-6} /°C close to the standard CTE (14.5×10^{-6} °C) of dentine Vita VMK 95 Dentine 1M2.

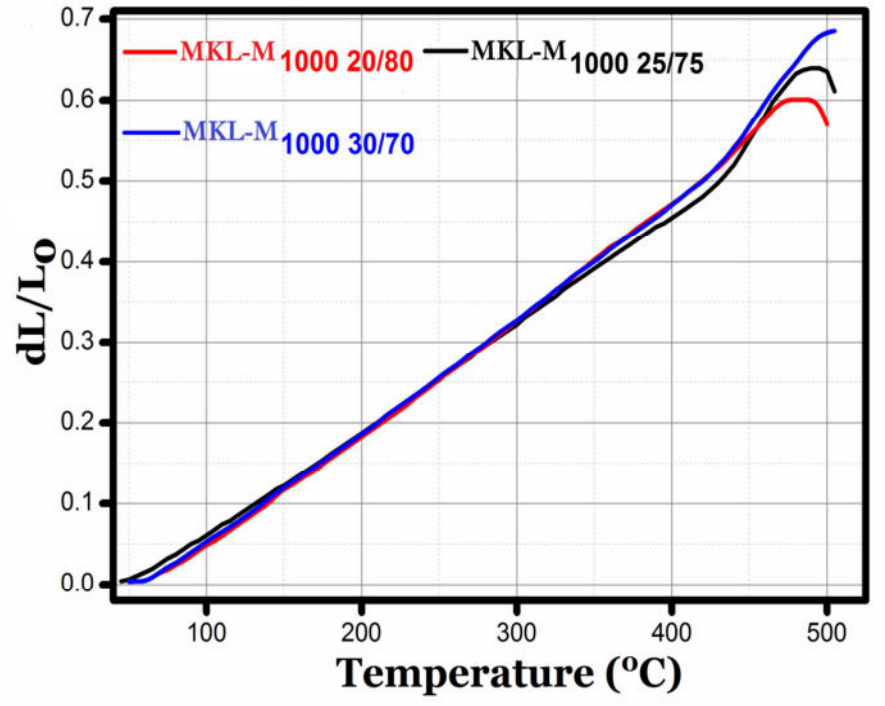

Fig. 4.16 CTE curves of the samples having different wt. % of kalsilite and LTF and 2 wt. % of MgF_2

4.2.3 Flexural strength

Fig. 4.17 shows the flexural strength of the MKL and MKL-M samples with different wt. % of kalsilite and LTF in the matrix. It is noted from Fig. 4.17 that flexural strength increases slightly with increasing the micro fine kalsilite in the matrix. The variation of kalsilite phase in the matrix is less (20-30 wt. % and remaining are LTF to match the CTE with standard nickel chrome alloy) leads to slight enhancement in the flexural strength for samples containing 20, 25 and 30 wt. % of kalsilite. The homogenous dispersion of nanocrystalline kalsilite grains within the glassy matrix leads to enhance the mechanical strength. It is also noted that MKL-M samples have slight increased flexural strength as compared to MKL samples. Therefore, it is claimed that addition of MgF_2 stabilizes the

kalsilite phase instead of leucite phase (as seen by XRD) however, it is not much affecting the flexural strength.

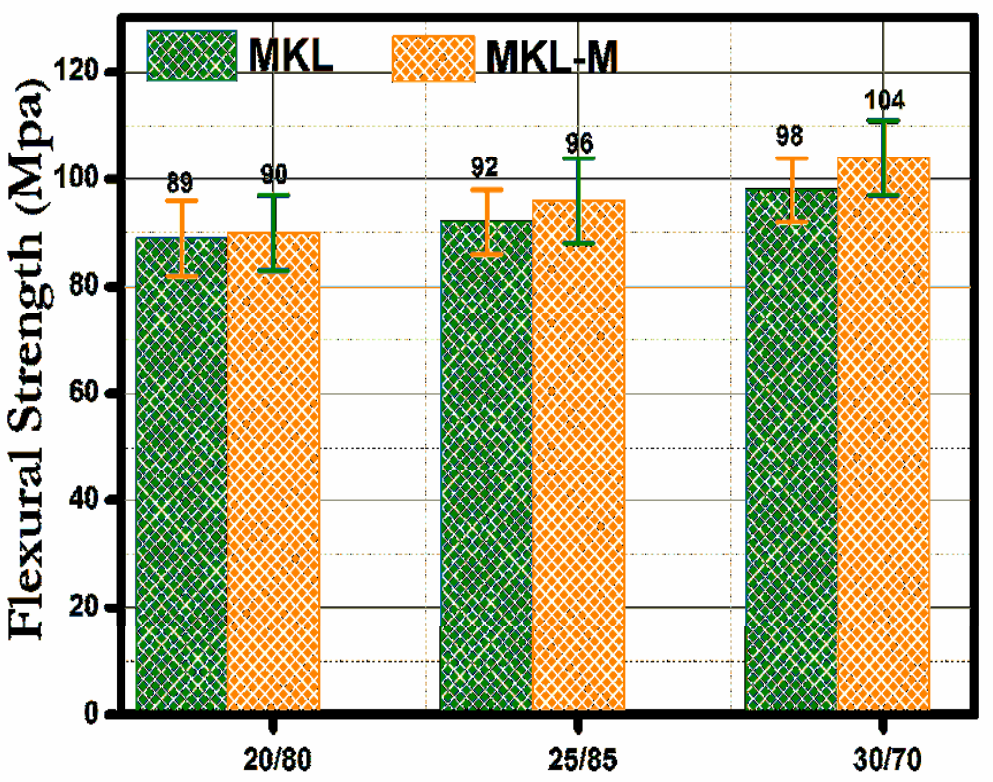

Fig. 4.17 Flexural strength of the MKL and MKL-M samples having different wt. % of kalsilite and LTF

4.2.4 Bulk density (BD) and apparent porosity (AP)

Fig. 4.18 shows the variation of BD and AP with wt. % of kalsilite in LTF portrayed. It is noted from Fig. 4.18 that BD increases with increasing the content of kalsilite followed by a continuous decrease in AP. This is due to dispersion of microfine kalsilite particles throughout the glassy matrix which improves the packing density of the samples.

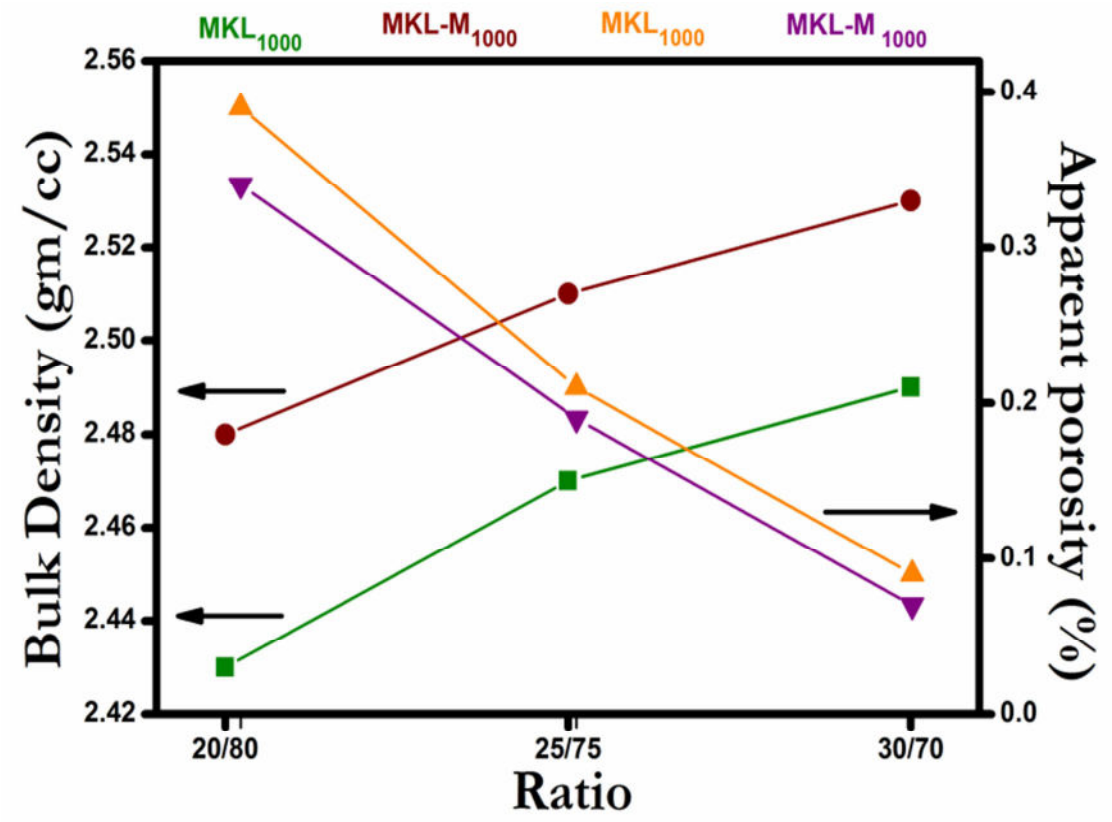

Fig. 4.18 BD and AP of samples contain different wt. % of kalsilite and LTF

4.2.5 Microstructure

The surface morphology of the MKL and MKL-M samples with different wt. % of LTF is shown in Figs. 4.19 & 4.20. The images show the homogenous distribution of hexagonal kalsilite throughout LTF matrix. There is no visible micro-crack appears due to the phase transformation. Micrographs show a very dense structure which is also in conformity with the AP and BD plots (Fig. 4.18).

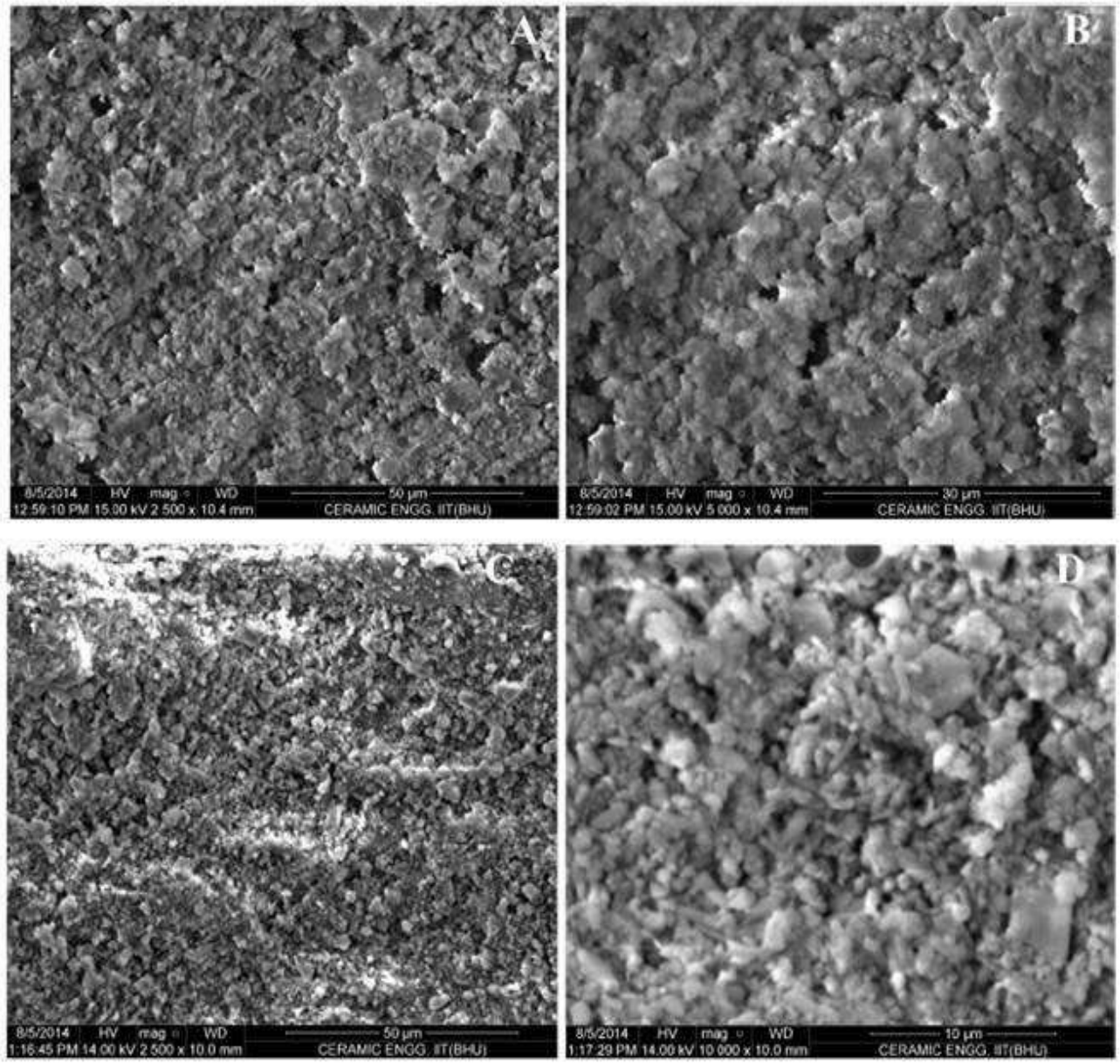

Fig. 4.19 SEM micrographs of the samples, MKL-$M_{1000\ 25/75}$ (A, B), MKL-$M_{1000\ 30/70}$ (C, D) at different magnification

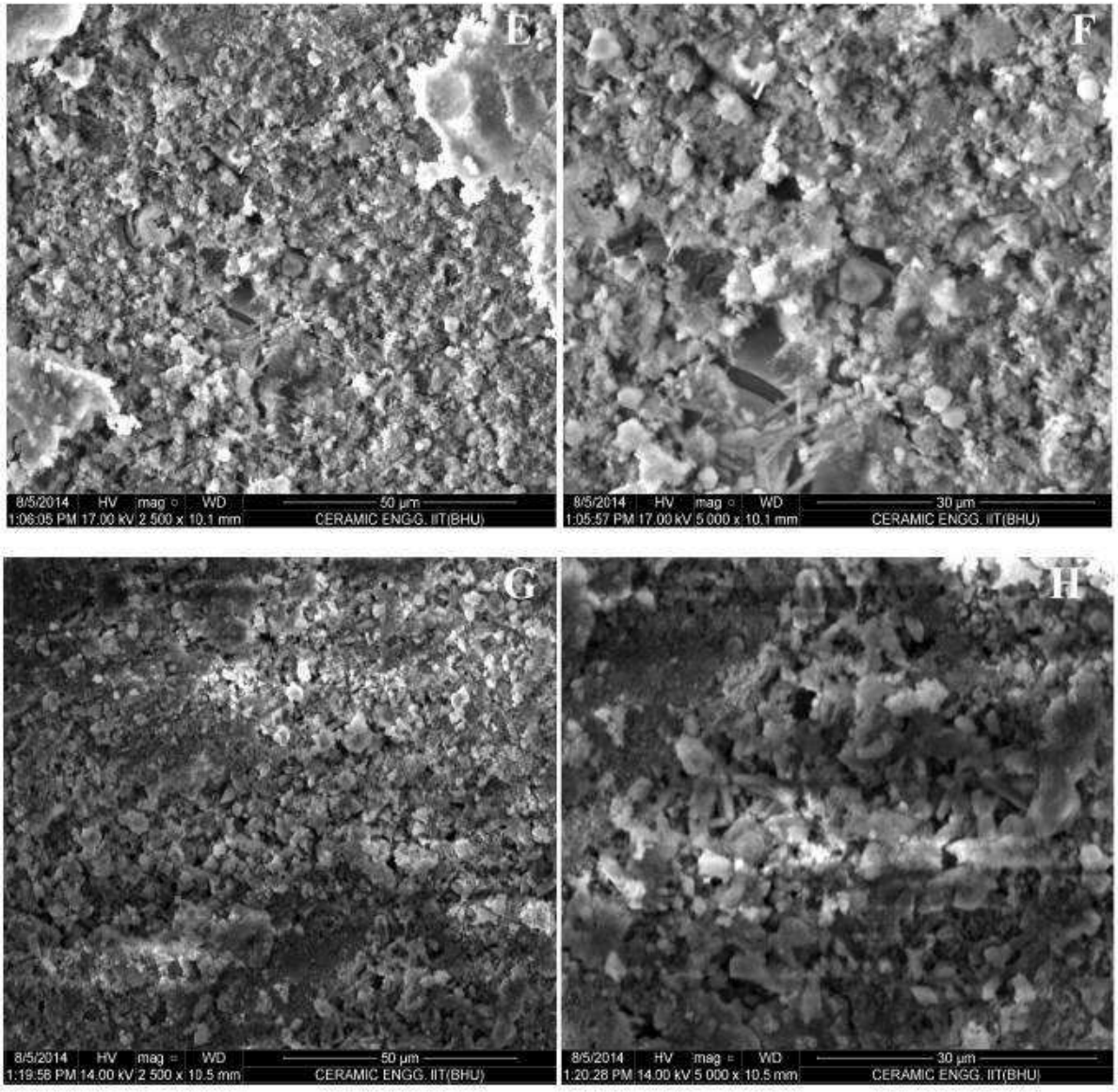

Fig. 4.20 SEM micrographs of the samples, $MKL_{1000\ 25/75}$ (E, F) and $MKL_{1000\ 30/70}$ (G, H) at different magnification

4.2.6 Ion leachability and surface morphology

Fig. 4.21 shows the weight loss of the kalsilite samples after immersion in 4% acetic acid and pineapple juice for 168 h. It is noted that weight loss of all the samples is less in the acetic acid than that in the pineapple juice. Weight loss decreases with increasing the content of fine kalsilite in the LTF matrix. This is due to the homogeneous distribution of

kalsilite throughout the matrix. MKL-M samples have slightly less weight loss than that of the MKL samples

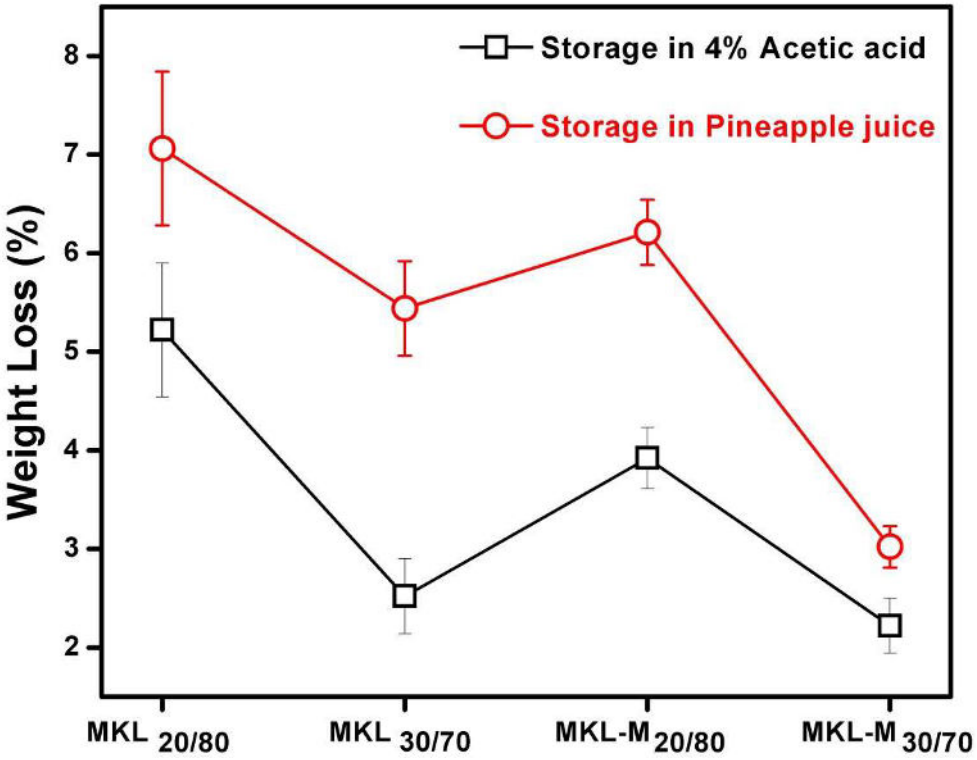

Fig. 4.21 Weight loss of MKL and MKL-M samples with different wt. % of LTF after immersion in 4% acetic acid and pineapple juice

The concentration of leached ions from the surface of kalsilite glass ceramics have been determined and reported in Table 4.4. In 4% acetic acid, the highest leaching values of sodium and potassium have been observed in $MKL_{20/80}$ and MKL-$M_{20/80}$. Similarly, in pineapple juice, the highest leaching values for these ions have been observed in $MKL_{20/80}$ and MKL-$M_{20/80}$. Furthermore, in both 4% acetic acid and pineapple juice, the lowest leaching values of sodium and potassium ions have been found in $MKL_{30/70}$ and MKL-$M_{30/70}$.

Table. 4.4 Leaching of ions from the kalsilite samples after immersion in 4% acetic acid and pineapple juice for 168 hours.

Leaching of ions from sample after immersion in storage agents for 0 and 168 hours	Storage agent	Time (hour)	Mean Ion leaching (µg/cm^2) (SD)		
			Na	K	Ca
$MKL_{20/80}$	4% Acetic acid	0	105 (8.1)	5 (0.3)	255 (13.6)
		168	4452.75 (254.41)	1868.18 (83.90)	1241.31 (78.63)
	Pineapple juice	0	185 (28)	5250 (102)	448 (16.5)
		168	316.64 (22.51)	7840.15 (384.92)	2654.71 (136.93)
$MKL_{30/70}$	4% Acetic acid	0	105 (8.1)	5 (0.3)	255 (13.6)
		168	3804.40 (219.66)	1825.66 (112.09)	1193.88 (82.66)
	Pineapple juice	0	185 (28)	5250 (102)	448 (16.5)
		168	220.56 (16.47)	7382.56 (221.66)	2418.22 (129.36)
MKL-$M_{20/80}$	4% Acetic acid	0	105 (8.1)	5 (0.3)	255 (13.6)
		168	2190.26 (116.44)	1838.45 (102.21)	1049.65 (95.11)
	Pineapple juice	0	185 (28)	5250 (102)	448 (16.5)
		168	261.24 (26.21)	6538.20 (233.42)	2118.6 (122.31)
MKL-$M_{30/70}$	4% Acetic acid	0	105 (8.1)	5 (0.3)	255 (13.6)
		168	1478.00 (105.67)	1674.92 (76.44)	983.36 (69.23)
	Pineapple juice	0	185 (28)	5250 (102)	448 (16.5)
		168	210.29 (26.09)	6896.23 (236.21)	1969.52 (101.52)

Fig. 4.22 shows the surface morphology of the kalsilite samples before immersion in acidic medium. The micrographs are very dense and have a glossy surface.

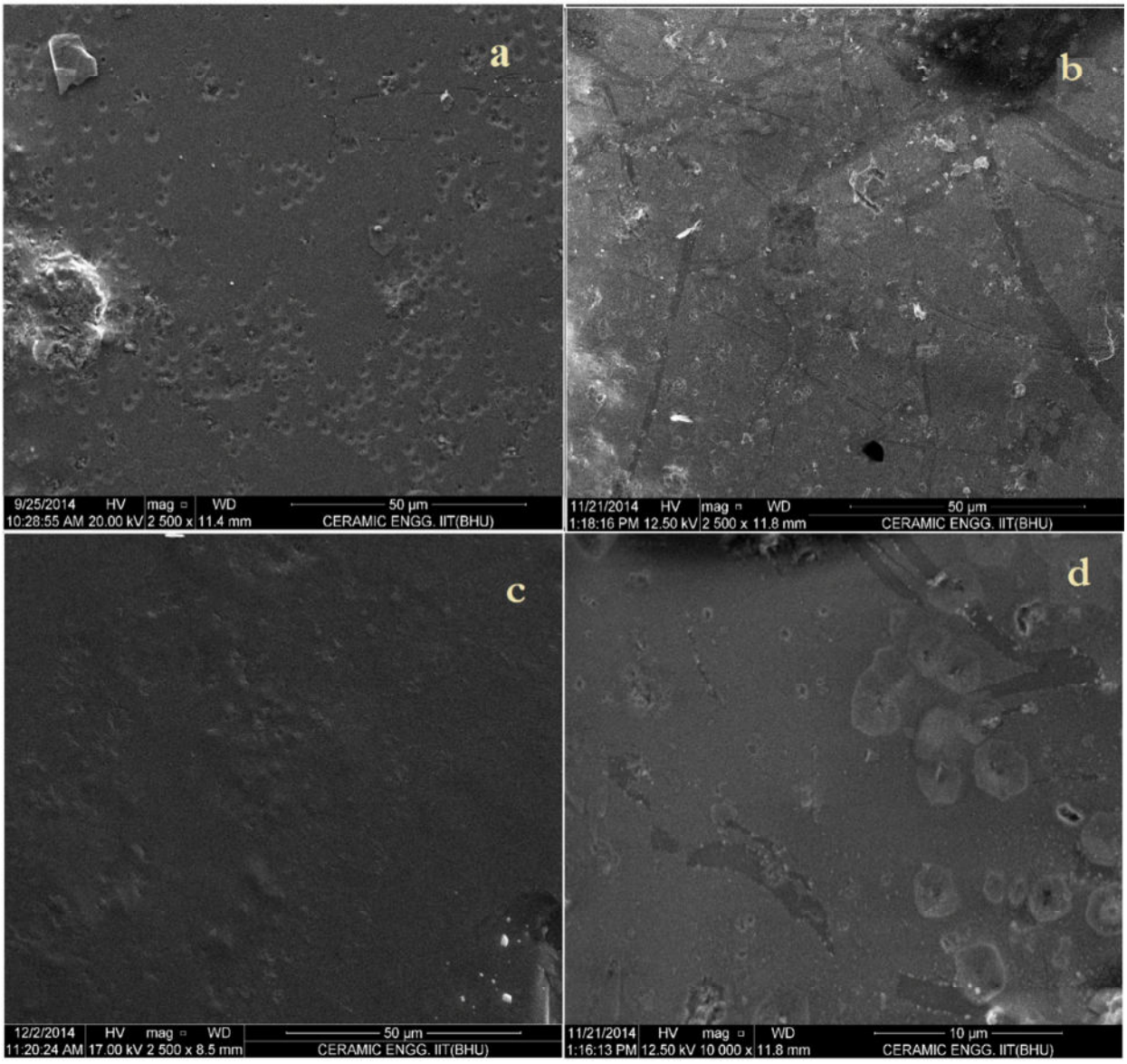

Fig. 4.22 SEM micrograph of the kalsilite samples before immersion in acidic medium) $MKL_{20/80}$; b) $MKL_{30/70}$; c) MKL-$M_{20/80}$ and d) MKL-$M_{30/70}$

Fig. 4.23 shows the surface morphology of the kalsilite samples after immersion in 4% acetic acid for 168 h. After immersion, the surface becomes rough and some open porosity portions have also been observed with the reduced glossiness. The maximum roughness and surface defects have been observed in the MKL samples and minimum in the MKL-M samples. It is also seen that the porosity and surface roughness decreases with increasing the kalsilite content in the LTF.

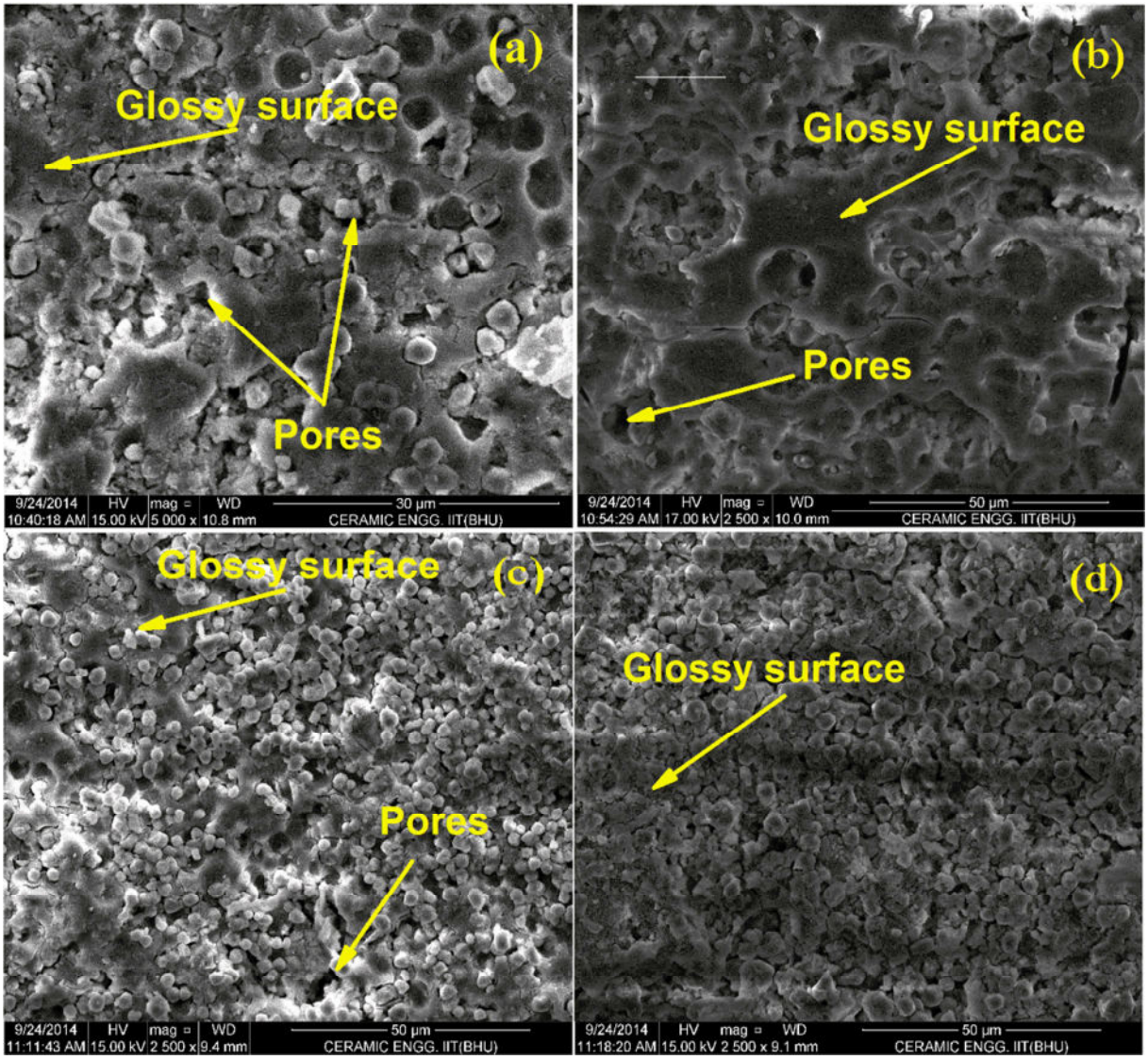

Fig. 4.23 SEM micrograph of the kalsilite samples after immersion in 4% acetic acid for 168 hours at 80 °C, a) $MKL_{20/80}$; b) $MKL_{30/70}$; c) MKL-$M_{20/80}$ and d) MKL-$M_{30/70}$

Fig. 4.24 shows the SEM micrographs of the MKL and MKL-M samples after immersion in pineapple juice for 168 h. It is noted that the surface roughness and defects are more as compared to that in Fig. 4.23 (after immersion in 4% acetic acid). This is also in conformity with the weight loss test that weight of all the samples is less in 4% acetic acid than that in the pineapple juice.

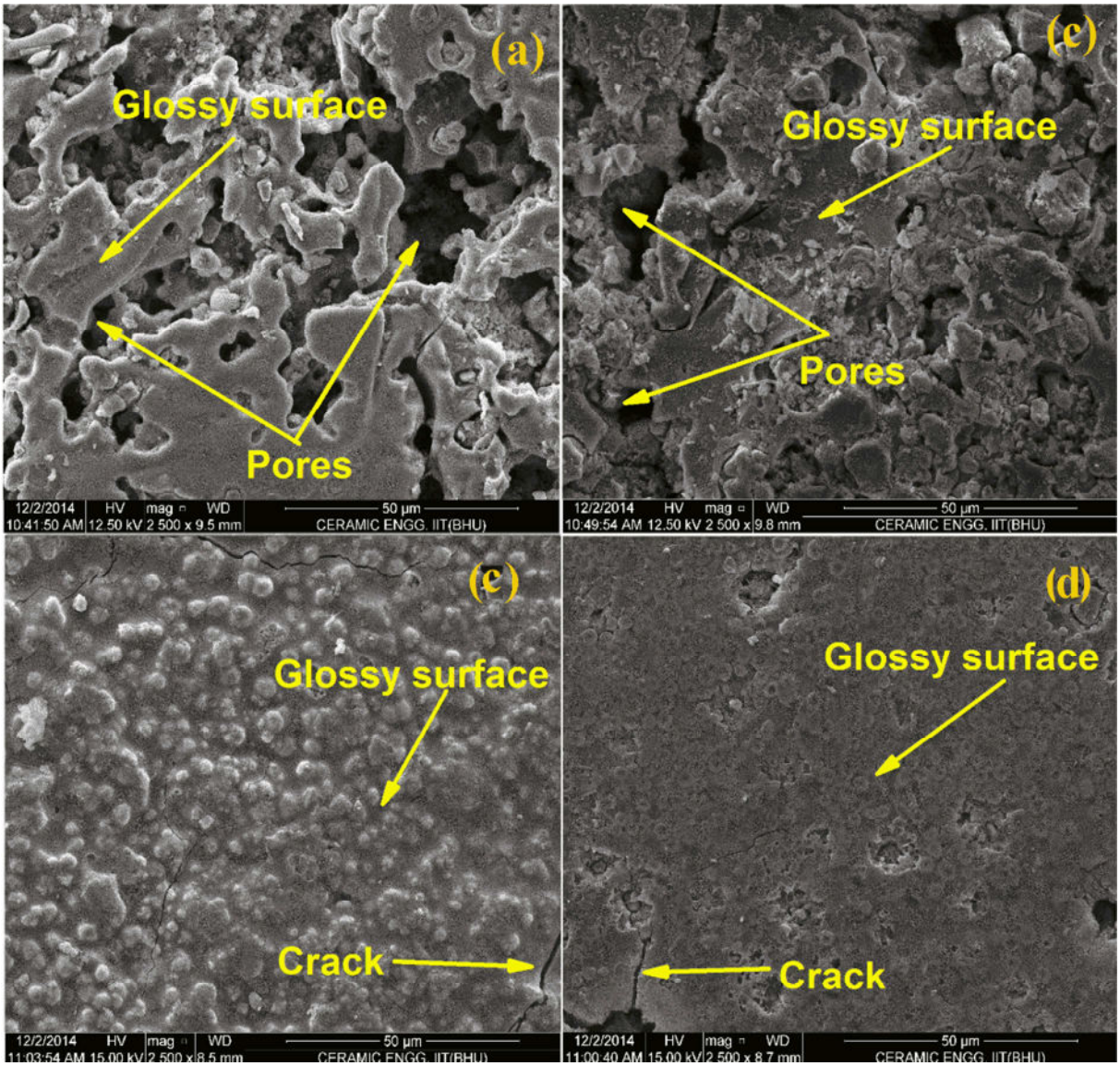

Fig. 4.24 SEM micrograph of the kalsilite samples after immersion in pineapple juice for 168 hours, a) $MKL_{20/80}$; b) $MKL_{30/70}$; c) $MKL\text{-}M_{20/80}$ and d) $MKL\text{-}M_{30/70}$

4.2.7 Summary of results

High enerfy ball milling has successfully synthesized kalsilite glass cermaic. The addition of MgF_2 suppresses the formation of leucite phase and stabilizes the kalsilite phase. Kalsilite with 2 wt. % of MgF_2 and containing different wt. % of LTF shows the CTE value in the range 14.0-14.8×10^{-6}/°C. This value is close to the standard CTE of (14.5 ×10^{-6}/°C) of dentine Vita VMK 95 Dentine 1M2. Samples containing higher wt. % of kalsilite have high flexural strength. This is due to the presence of micro fine kalsilite particles in the matrix. Micrographs show a very dense structure with no visible cracks. Therefore, this material is a potential candidate for PFM. MKL samples have high ion leachability than that of the MKL-M samples. This is also in conformity with the flexural strength i.e. MKL-M samples have slight higher flexural strength than that of the MKL samples. The leaching of Na^+ and K^+ is more in the acetic acid and pineapple juice respectively. Compositions, MKL_{1000} and MKL-M_{1000} show the better properties among the series, therefore, these compositions have been selected for determination of their bioactive properties.

4.3 Mechanochemically Synthesized leucite/kalsilite based bioactive glass ceramic composite for dental veneering

4.3.1 Phase analysis

Phase formation in the leucite and kalsilite composites has been confirmed using XRD. Figs. 4.25 & 4.26 show the XRD patterns of the leucite glass ceramic composites with & without CaF_2 before and after heat treatment. Before heat treatment, diffraction peaks are well matched to the JCPDS card No. 71-1147 of leucite with the unit cell parameters a = b =13.09 and c = 13.75 Å (Figs. 4.25 & 4.26).

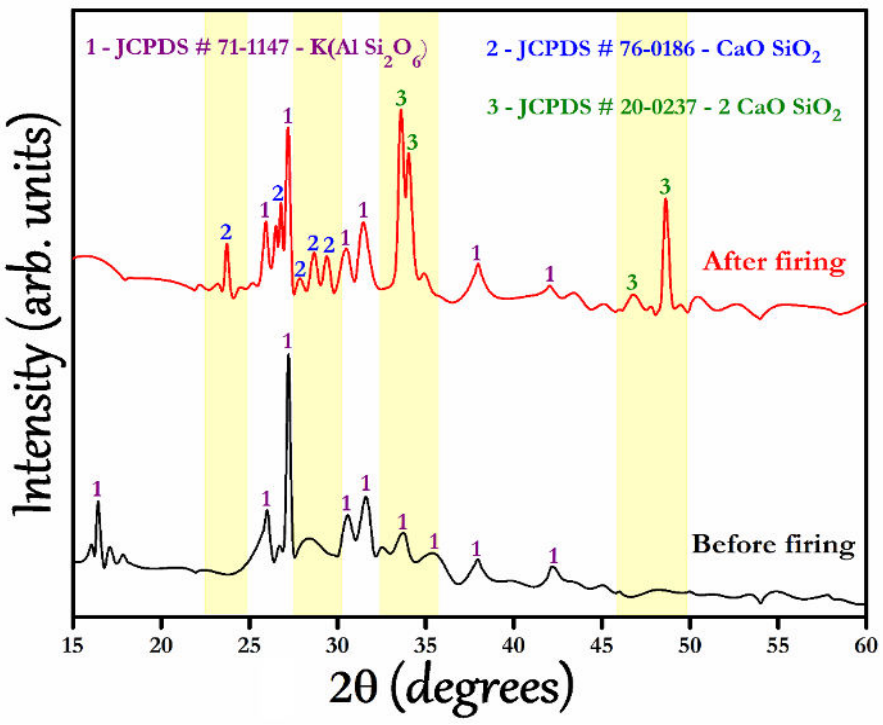

Fig. 4.25 XRD pattern of COMP-1 before and after heat treatment up to 960 °C

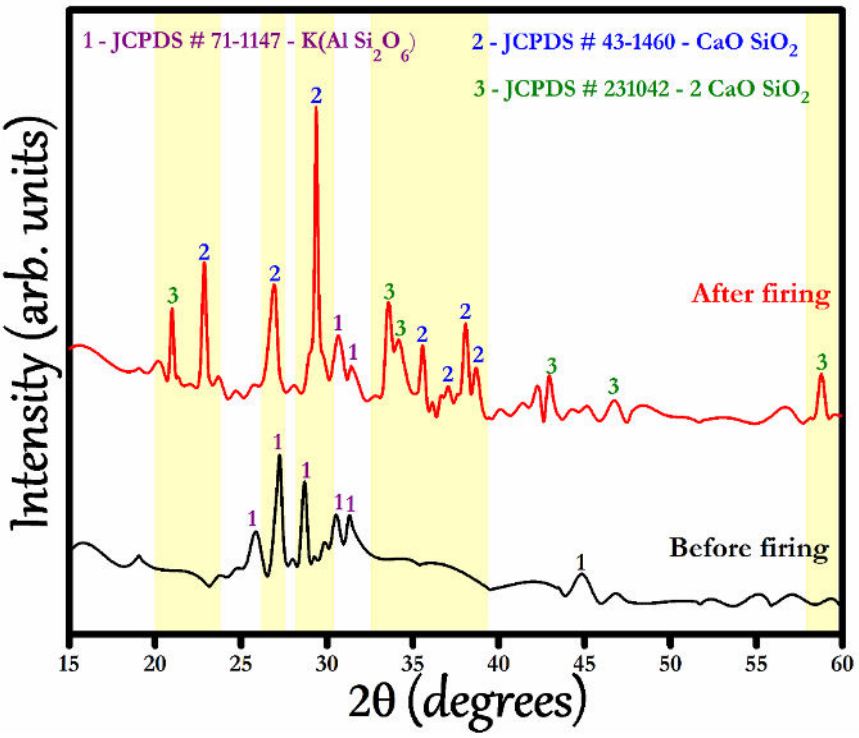

Fig. 4.26 XRD pattern of COMP-2 before and after heat treatment up to 960 °C

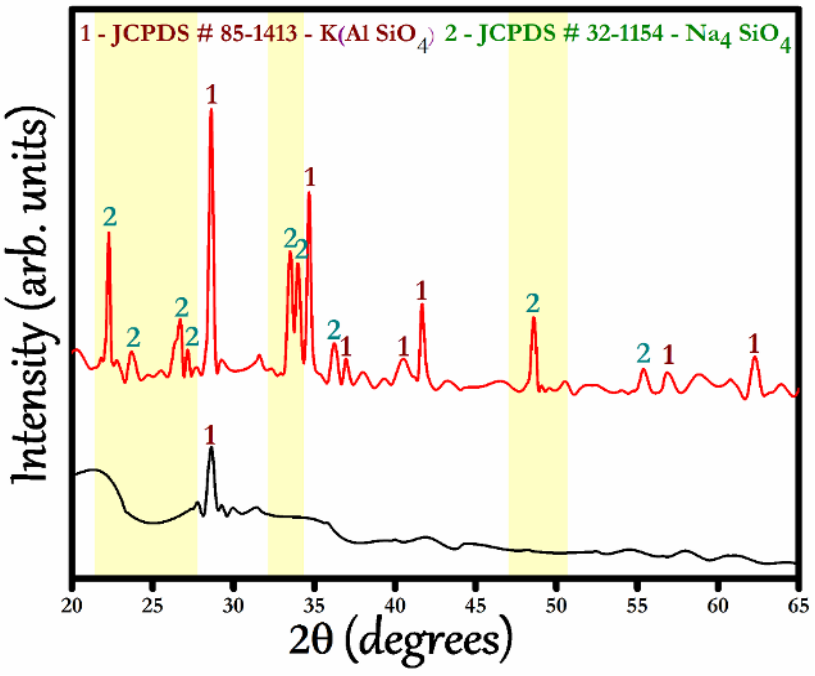

Fig. 4.27 XRD pattern of COMP-3 before and after heat treatment up to 960 °C

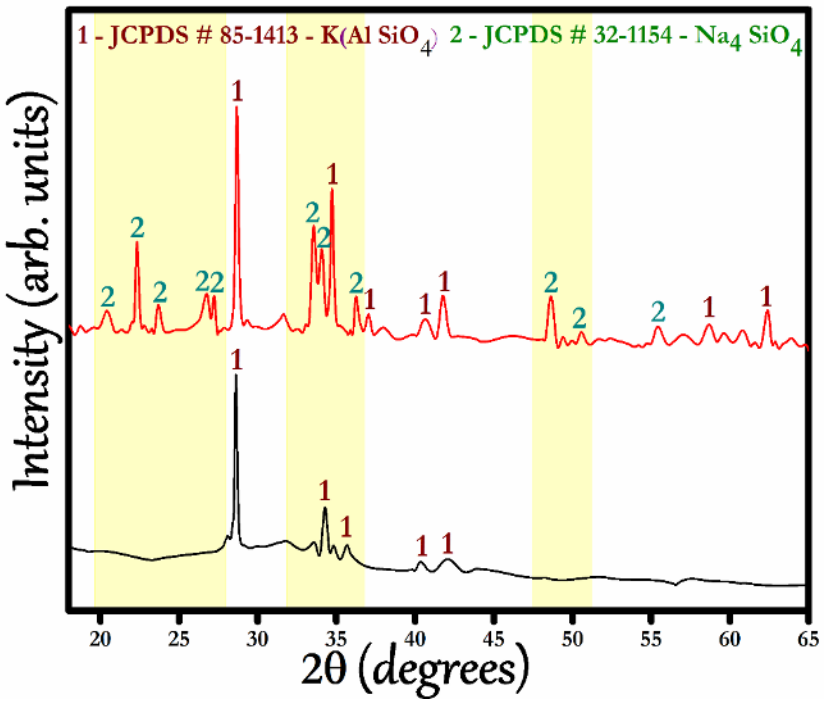

Fig. 4.28 XRD pattern of COMP-4 before and after heat treatment up to 960 °C

It is noted from Fig. 4.25 & 4.26 that after heat treatment, a calcium silicate ($2CaO.SiO_2$) and wollastonite ($CaO.SiO_2$) crystalline phases has been observed in both the leucite composites (COMP-1 & COMP-2). The Intensity of the peaks corresponding to leucite phase has been reduced after heat treatment accompanying with the formation of another two phases, calcium silicate and wollastonite. It is also seen from Fig. 4.26 that formation of wollastonite phase is higher in the case of COMP-2 (after heat treatment) than that of COMP-1. Formation of the $2CaO.SiO_2$ and $CaO.SiO_2$ crystalline phases may lead to improving the flexural strength. This is because these phases have high flexural strength.

Figs. 4.27 & 4.28 show the XRD patterns of the kalsilite glass ceramic composites with & without MgF_2 (before and after heat treatment). Before firing, the diffraction peaks are well matched to the JCPDS card No. 85-1413 of kalsilite phase. Some amorphous phase is also seen in the XRD patterns. After firing, a sodium orthosilicate ($2Na_2O.SiO_2$) crystalline phase has been found in both the composites (COMP-3 & COMP-4) along with the kalsilite phase.

4.3.2 Coefficient of thermal expansion (CTE)

Thermal compatibility is the most essentials for veneering glass-ceramic fused to metal restorations. Fig. 4.29 shows the thermal expansion behavior of all the leucite and kalsilite bioactive glass ceramic composites along with the commercial Dentine A2.

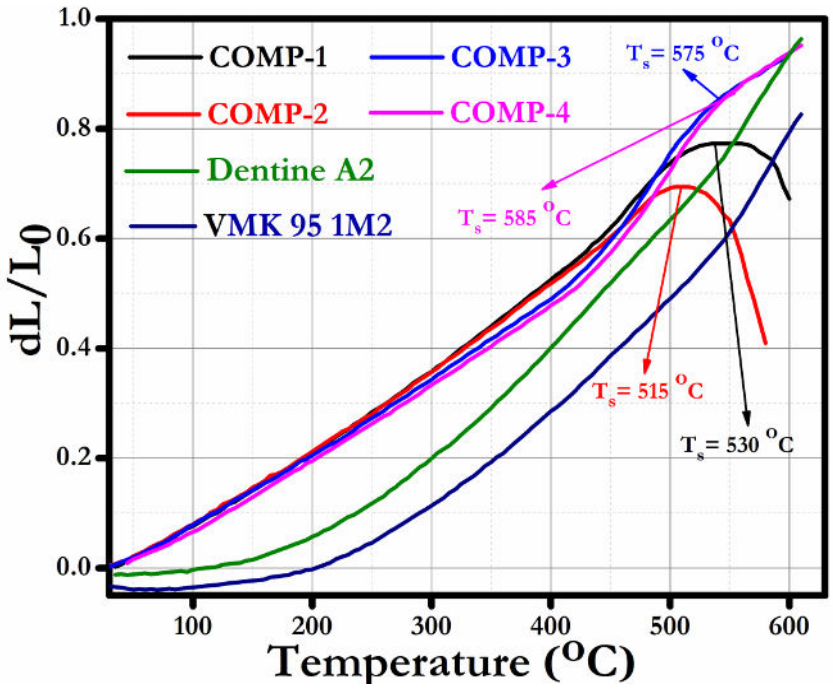

Fig. 4.29 CTE curves of COMP-1, COMP-2, COMP-3 and COMP-4 along with commercial Dentine A2 and substrate

The values of CTE have been found to be 15.6×10^{-6}, 14.5×10^{-6}, 15.9×10^{-6} and 15.6×10^{-6} /°C for the samples COMP-1, COMP-2, COMP-3 and COMP-4 respectively.

These values are similar to the values obtained for dentine (VITA VMK 95 Dentin 1M2) and the opaque layer (VITA VMK95 opaque 1M2) as 14.5×10^{-6} /°C & 14.0×10^{-6}/°C respectively. The values of CTE for both the substrate and the composite are very close therefore applied heat treatment will not lead to peel off the coating. The composition COMP-2 has slightly low CTE than that of COMP-1. It is because of that more Ca^{2+} ions enter into leucite lattice at high temperature and lower the CTE [Zhang Y. *et al.* 2006]. Leucite and kalsilite have a high CTE value, therefore, increase the overall thermal expansion of the dental ceramic compatible with the metals [Hashimoto S. *et al.* 2005].

4.3.3 Flexural strength

Fig. 4.30 shows the flexural strength of all the composites and commercial dentine A2. The prepared composite samples show the flexural strength comparable to that of the commercial dentine. This is due to the formation of the crystalline calcium silicate and wollastonite phases (after heat treatment) in the leucite based composites and sodium orthosilicate in the kalsilite based composites. It is noted from Fig. 4.30 that the composition COMP-2 has the high flexural strength than that of COMP-1. This is in conformity with the CTE results that COMP-2 has low CTE than that of COMP-1. It leads to increase in the flexural strength.

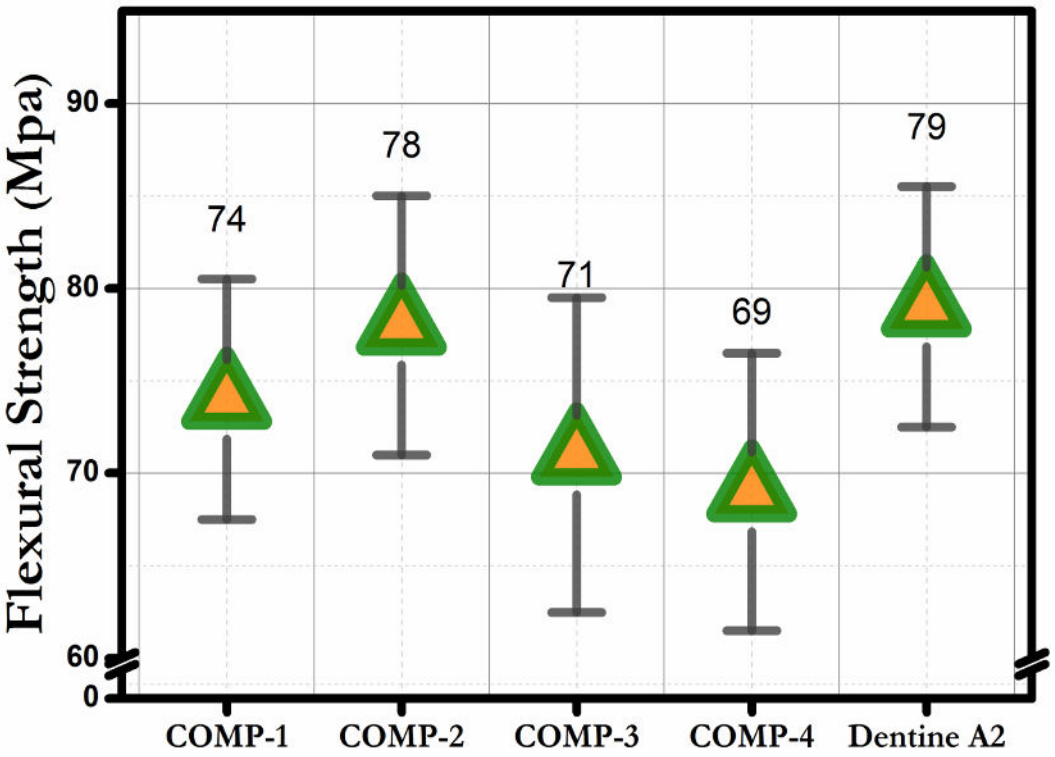

Fig. 4.30 Flexural strength of COMP-1, COMP-2, COMP-3, COMP-4 and commercial dentine

Composition COMP-3 and COMP-4 has the low flexural strength than that of COMP-2. This is because sodium orthosilicate ($2Na_2O.SiO_2$) has less strength as compared to the calcium silicate and wollastonite [Al-Noaman A. *et al.* 2013].

It is also noted that composition, COMP-4 has less flexural strength than that of the COMP-3. This is because the concentration of sodium orthosilicate phase is slightly higher in COMP-4 than that in the COMP-3 (Figs. 4.27 & 4.28). This leads to decrease in the flexural strength of COMP-4.

4.3.4 Interface layer of the composites and the substrate

Fig. 4.31 shows the surface morphology of the interface layer between the composite and the substrate (composite coated substrate). It confirms a perfect attachment between the substrate and the composite coating. There is no micro crack and peeling throughout the interfaces. Compression interface bond depends on the geometry of CTE of the substrate. The firm attachment of the bioactive coating on the substrate has been ascribed to the well matched CTE.

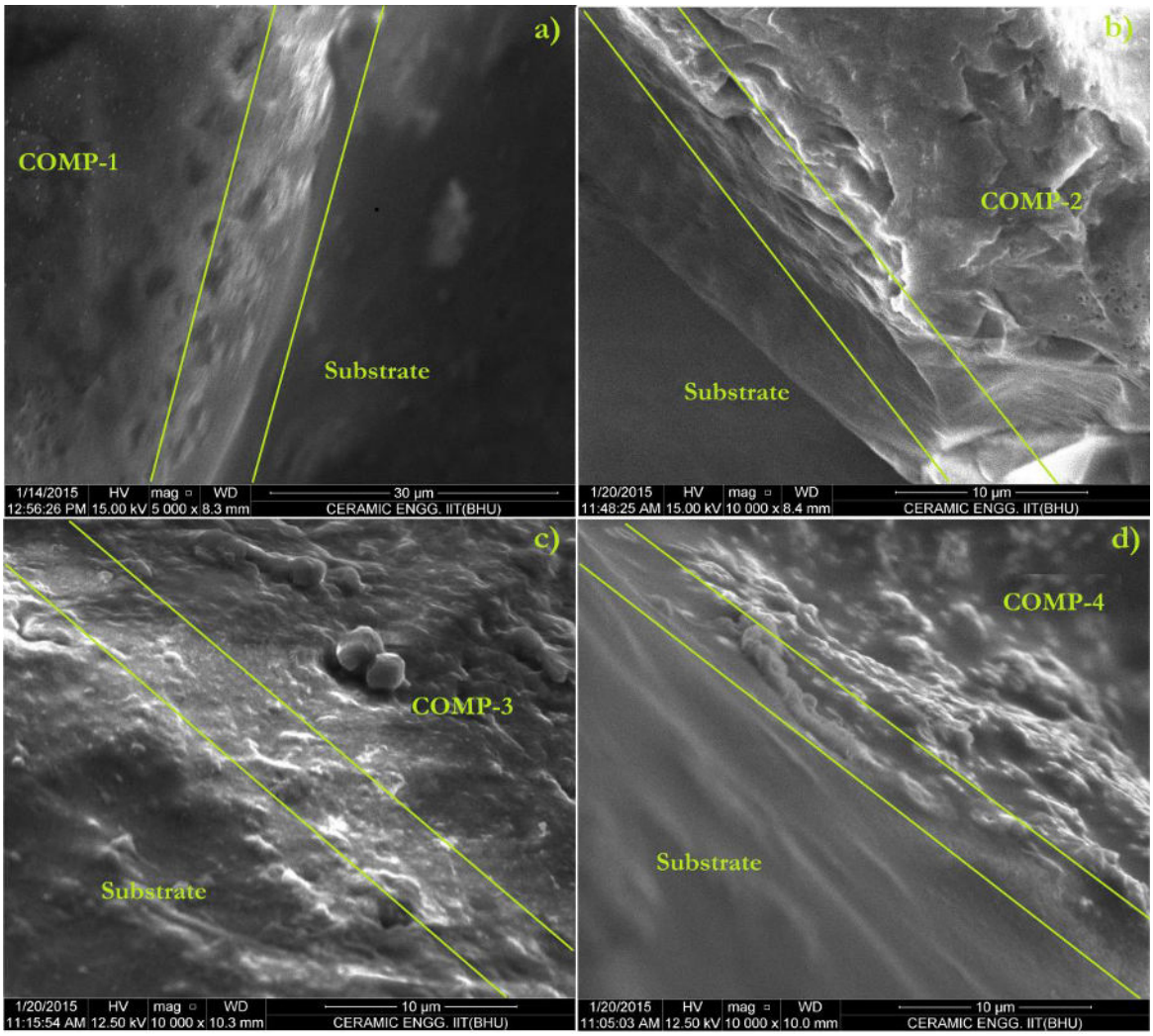

Fig. 4.31 SEM image showing the surface morphology of interface layer between the composites and the substrate

4.3.5 Bioactivity in SBF

The capability of hydroxyapatite layer formation has been investigated on the bioactive glass ceramic composites through immersion in SBF for 0, 7 and 14 days soaking time.

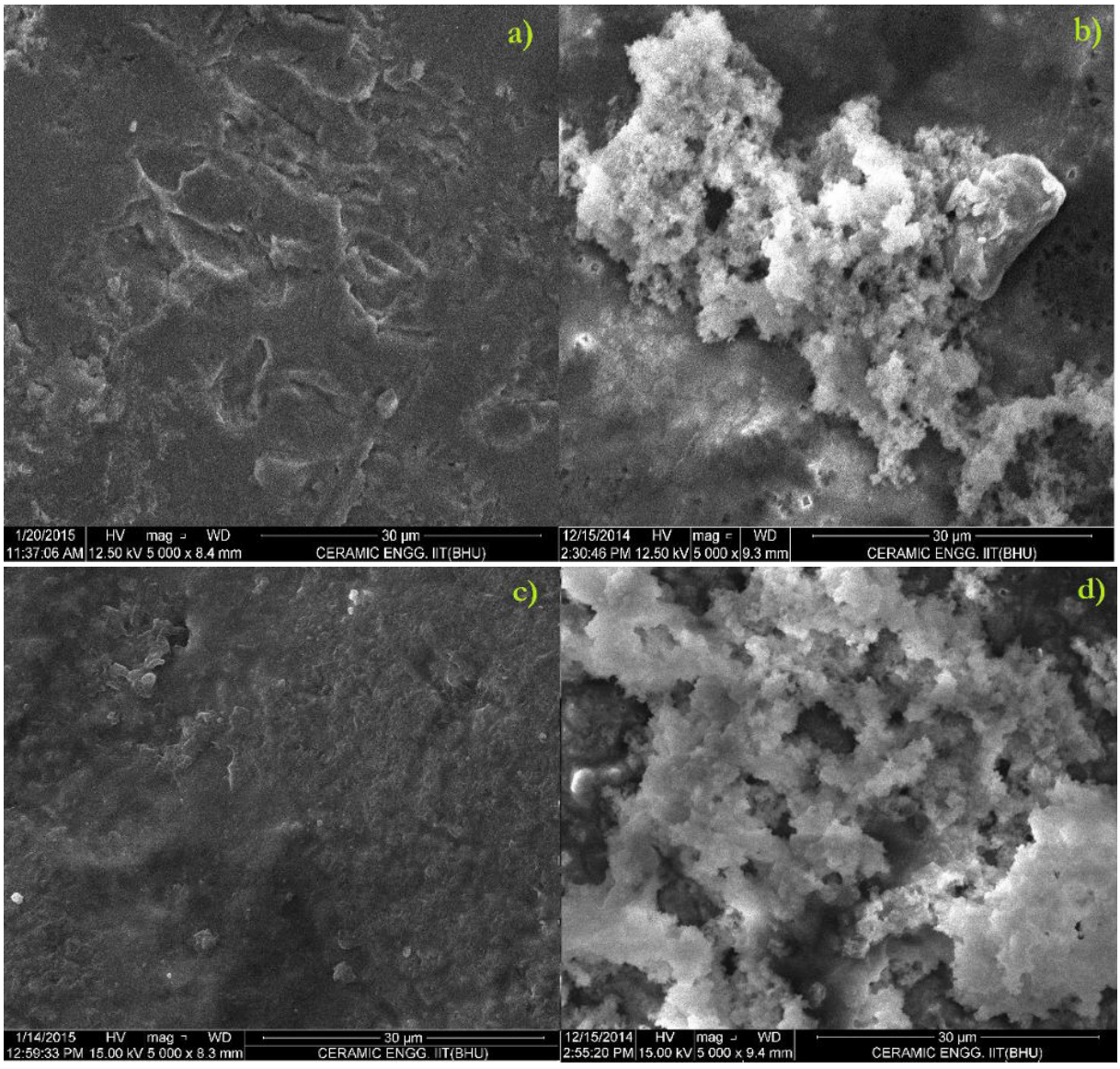

Fig. 4.32 SEM images of the coated specimens of COMP-1 (a) before (b) after immersion for 7 days in SBF, COMP-2 (c) before and (d) after immersion for 7days in SBF showing HAp formation

The surface of the specimens before and after immersion in SBF has been examined by SEM (Fig. 4.32). The hydroxyapatite layer covers the whole surface of all the composite samples, has been observed after 7 days soaking in SBF (Fig. 4.32a to 4.32h). FTIR has analyzed all composite samples soaked in SBF.

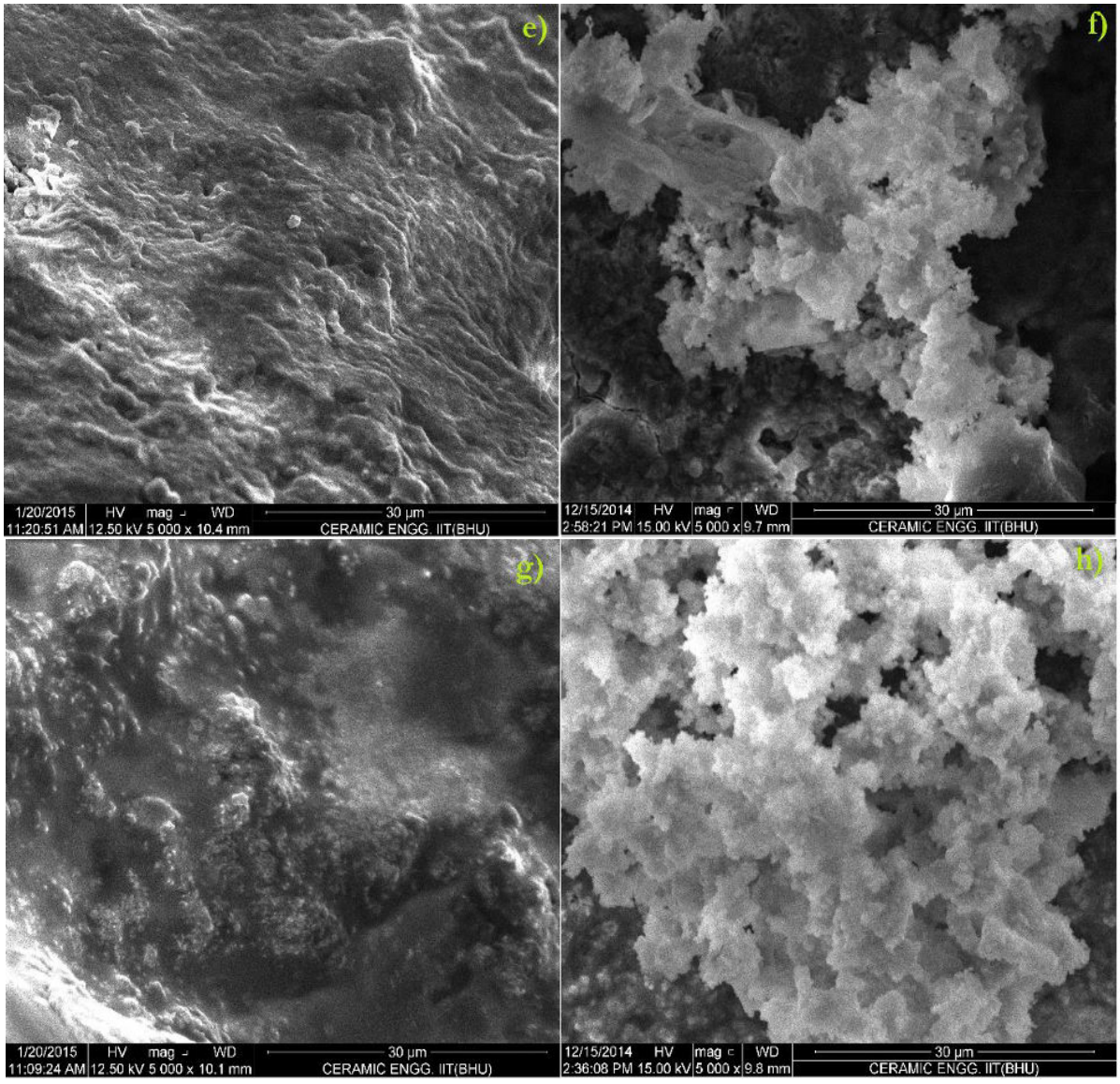

Fig. 4.32 SEM images of the coated specimens of COMP-3 (e) before and (f) after immersion for 7 days in SBF showing HAp formation, COMP-4 (g) before and (h) after immersion for 7 days in SBF showing HAp formation

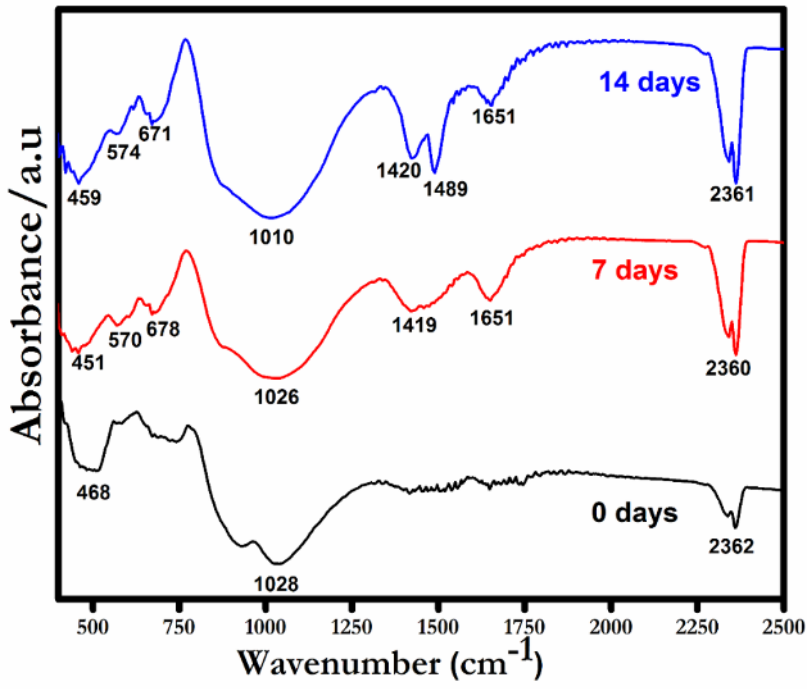

Fig. 4.33 FTIR absorbance bands of COMP-1 composite before and after immersion in SBF for 0, 7 and 14 days

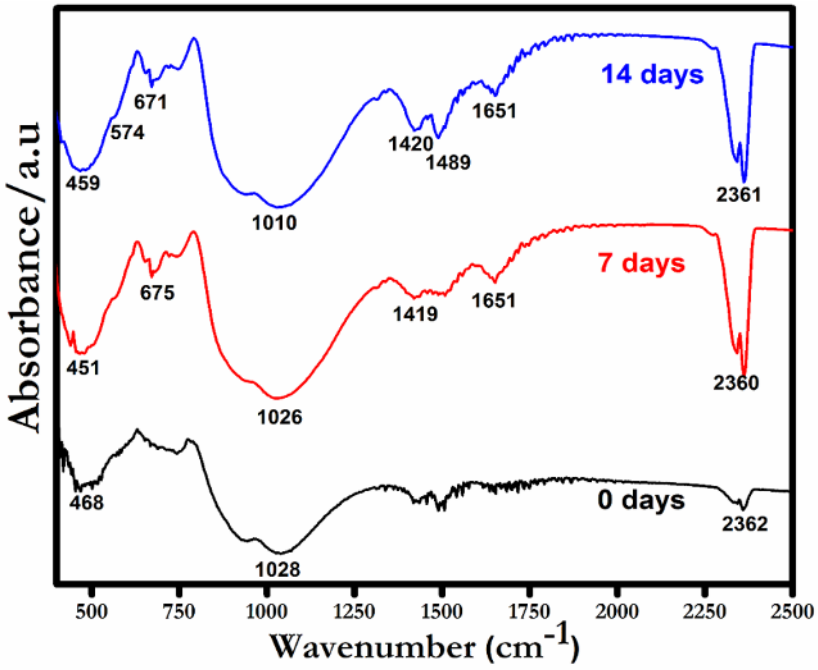

Fig. 4.34 FTIR absorbance bands of COMP-2 composite before and after immersion in SBF for 0, 7 and 14 days

Figs. 4.33 to 4.36 show the FTIR transmittance bands of the composites before and after immersion in SBF for 0, 7 and 14 days. Intense peaks in the wavelength range 1150–900 and 650–500 cm^{-1} is observed due to stretching vibrations of the phosphate (PO_4^{-3}) groups (after soaking in SBF for 7 days at 37 °C). The low intense peaks appeared in the range 1500–1400 cm^{-1} indicates the presence of CO_3^{-2} molecules in the sample.

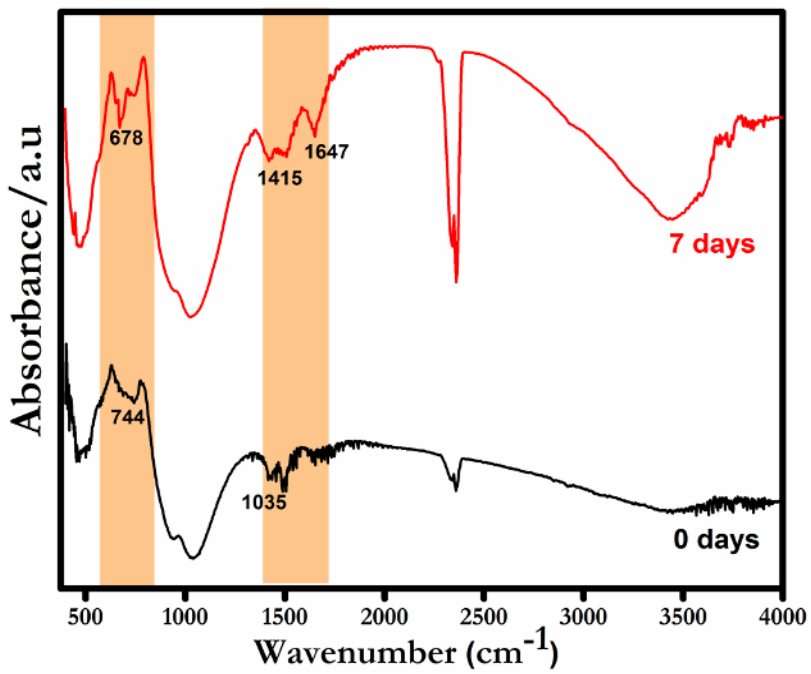

Fig. 4.35 FTIR absorbance bands of COMP-3 composite before and after immersion in SBF for 0 and 7 days

There is also an additional peak at 450 cm^{-1} assigned to the bending vibration mode of Si-O bond. The results of SEM are also in conformity with the results of FTIR. Since in the 1990s, wollastonite ($CaSiO_3$) ceramics have been studied as biomaterials for artificial bones and dental roots because wollastonite exhibits excellent bioactivity and biocompatibility. Some investigators have been reported that wollastonite and pseudo-wollastonite ceramics are bioactive and observed that the formation of apatite on the

$CaSiO_3$ ceramics is faster than that on the other bioglass and glass-ceramics in SBF [Noaman A.A. *et al.* 2013].

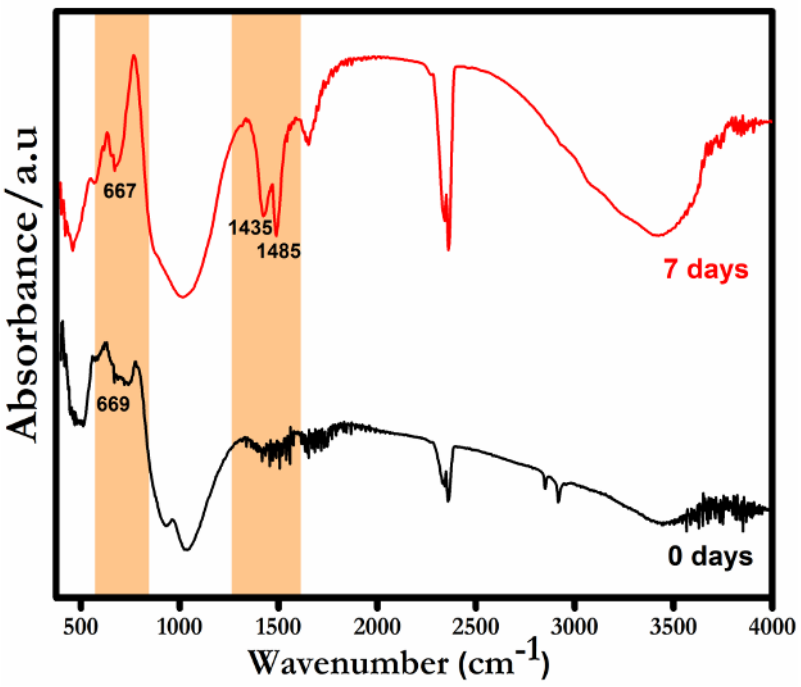

Fig. 4.36 FTIR absorbance bands of COMP-4 composite before and after immersion in SBF for 0 and7 days

Siriphannon et al. have reported that the rate of hydroxyapatite (HA) formation on the pure $CaSiO_3$ ceramic surface is faster than that on the biocompatible apatite-wollastonite A/W glass-ceramics and some other bioactive glass-ceramics [Siriphannon P. *et al.* 1999].

4.3.6 Effect of composite materials on viability and cellular growth inhibition

Higher concentrations of leucite and kalsilite glass-ceramic composites causes partial loss of cell viability in SCC-25 cells although lower concentrations of all the compounds are relatively tolerant to the cells (Fig. 4.37 A). At 10 mg/ml, the cell viability is recorded around 80% and reduces with increasing the concentration (Fig. 4.37 A). A moderate level of growth inhibition has also been observed in SCC-25 cells with the compound of higher concentrations while low concentrated compounds are found to be safe and have no effect on cellular proliferation (Fig. 4.37 B). This suggests a broad spectrum usefulness of the compounds (Fig. 4.37 B). Growth inhibition with kalsilite glass ceramic materials at a fixed concentration (10 mg/ml) for longer periods (72h) causes a moderate retardation (20%) of cell growth compared to treatment for 18h (Fig. 4.37 C).

Interestingly prepared composite materials to perform better as compared to the standard material on inhibition of cell proliferation (Fig. 4.37 C). The direct cellular cytotoxicity test has also been performed with leucite and kalsilite glass–ceramic composites against SCC-25 cells (Fig. 4.37 D). As compared to the higher concentration (50 mg/ml), the low concentrations of leucite and kalsilite glass–ceramic composites are tolerant to the SCC-25 cells and causes significantly less celllysis (Fig. 4.37 D). The results show that leucite and kalsilite glass–ceramic composites are cytocompatible and relatively nontoxic to buccal epithelial cells.

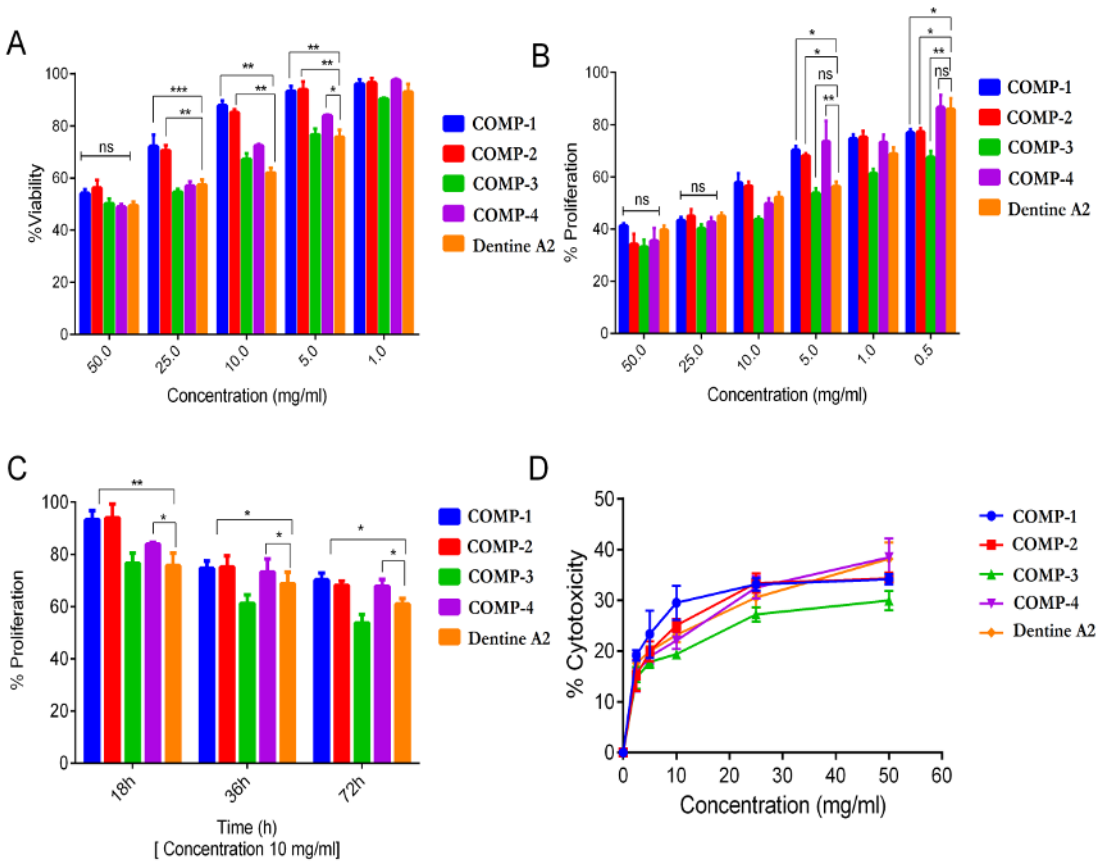

Fig. 4.37 Higher concentration of composite materials retards the growth of SCC-25 cells. (A) The viability of SCC-25 cells in the presence of COMP-1, COMP-2, COMP-3 and COMP-4 glass–ceramic composites (B&C) Graphs show concentration response of leucite and kalsilite glass–ceramic composite materials on tumor cell proliferation and growth (D) Direct cellular cytotoxicity by composite materials against SCC-25 cells. Data presented as mean ± SD, n = 4. * p<0.5, ** p<0.01, *** p<0.001

4.3.7 Apoptosis study

Growth inhibition by leucite and kalsilite glass–ceramic composites at higher concentration raises the question whether it also causes apoptosis of the tumor cells and if so whether it induces cell death. Apoptosis has been determined by monitoring the changes in the cell size and externalization of phosphatidylserine qualitatively in SCC-25 cells [Manna P.P. *et al.* 2013].

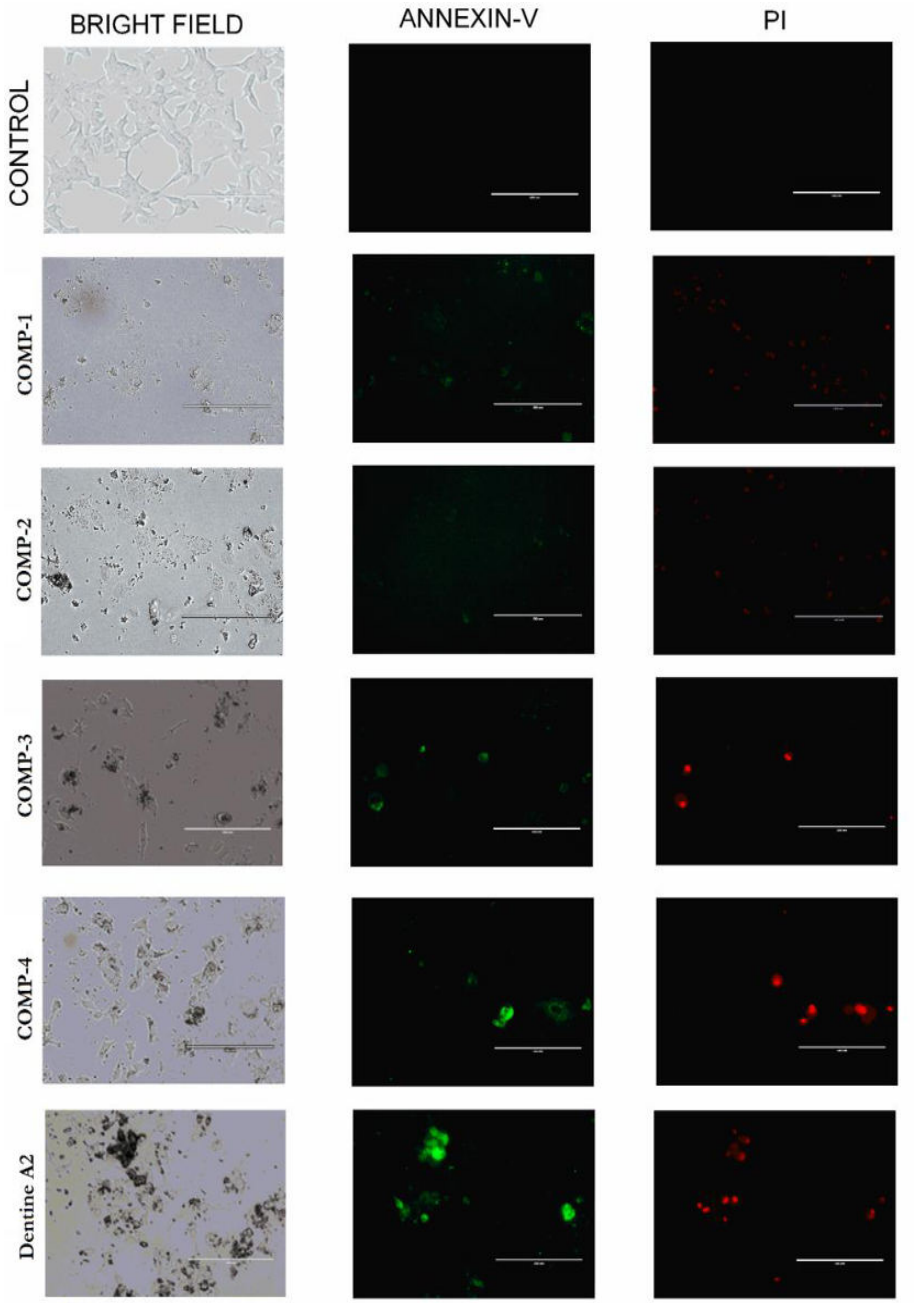

Fig. 4.38 Microscopic analysis of induction of apoptosis SCC-25 cells were given indicated treatment with COMP-1, COMP-2, COMP-3 and COMP-4 glass–ceramic composites materials at a concentration of 50mg/ml in complete RPMI 1640 medium for 8h at 37 ^{o}C. FITC-conjugated Annexin V and Propidium iodide (PI) stained apoptotic cells were visualized under a fluorescence microscope (Nikon Eclipse 80i, Nikon, Japan) with Plan Fluor, 40X, NA 0.75 objective equipped with green and red filters for FITC and PI, respectively. n=3

There is a moderate increase in Annexin V positive cells upon treatment with compositions COMP-3 & COMP-4 (50 mg/ml) and the standard (STD) (Fig. 4.38). The other composite material causes no apoptosis in SCC-25 cells (Fig. 4.38).

4.3.8 Culture of SCC-25 cells on leucite and kalsilite glass–ceramic composites

SCC-25 cells have been cultured on the leucite and kalsilite glass–ceramic composites to demonstrate both the cytocompatibility and biocompatibility of the compounds in the case of clinical application. It has been observed that leucite and kalsilite based glass–ceramic composites are tolerant to the growth of the SCC-25 cells. This is consistent with our results as observed concerning growth inhibition and cytotoxicity (Figs. 4.39-4.43).

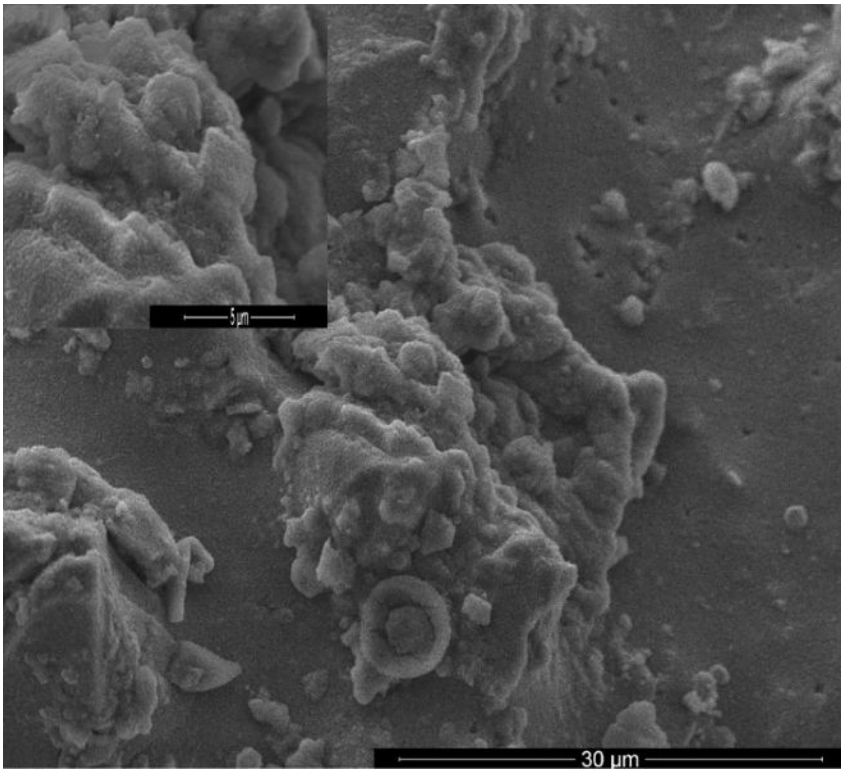

Fig. 4.39 SEM images of the surface of COMP-1showing the proliferation and spreading of SCC-25 cells after 10 days of culture on COMP-1 glass–ceramic composites (image at same magnification and scale bar represent 30µm (inset)

The results also suggest that the prepared composite materials perform better as compared to the standard materials and allow efficient growth of the cells over its surface (Figs. 4.39-4.42).

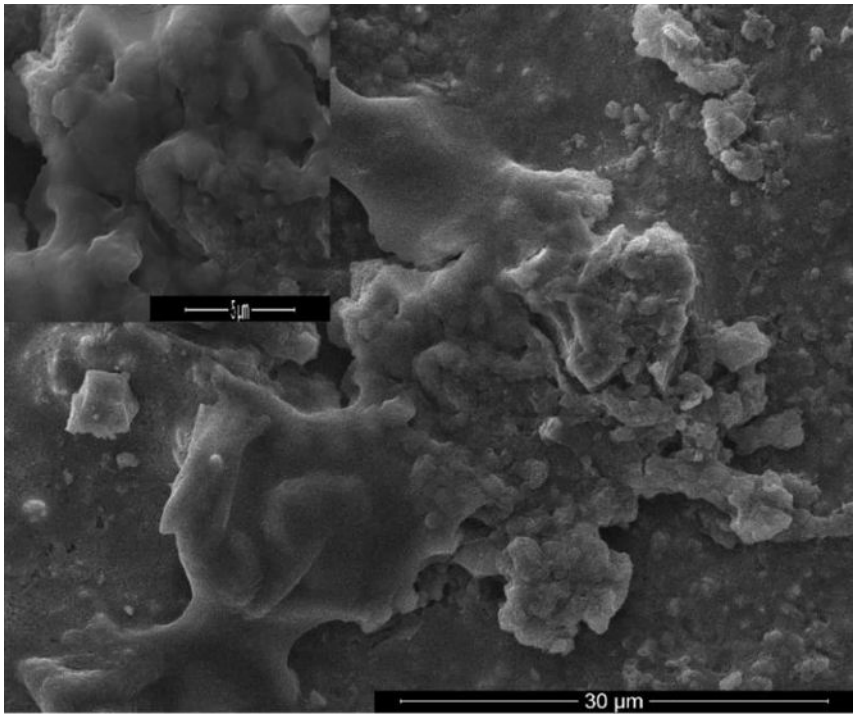

Fig. 4.40 SEM image of the surface of COMP-2 showing the proliferation and spreading of SCC-25 cells after 10 days of culture on COMP-2 (image at same magnification and scale bar represent 30µm (inset)

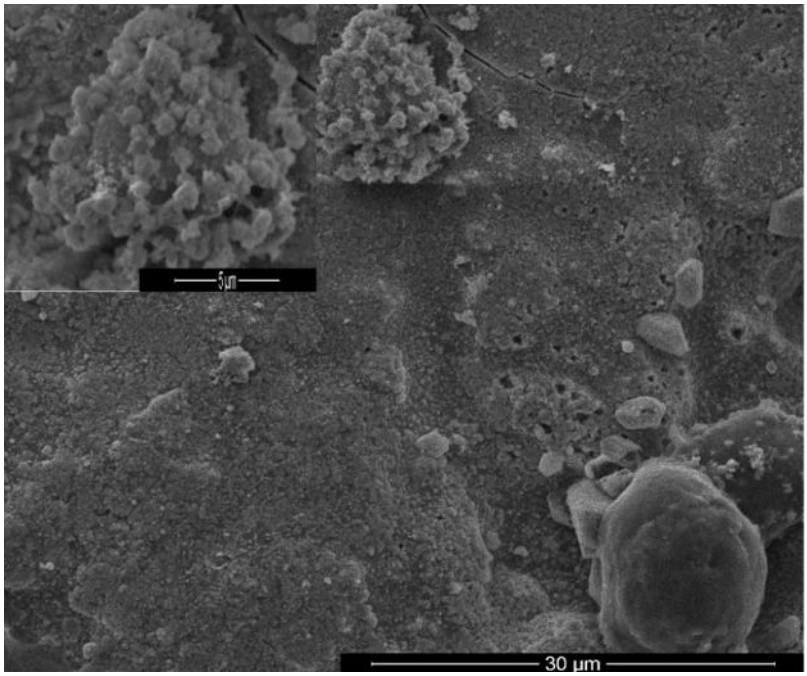

Fig. 4.41 SEM image of the surface of COMP-3 showing the proliferation and spreading of SCC-25 cells after 10 days of culture on COMP-3 (image at same magnification and scale bar represent 30µm (inset)

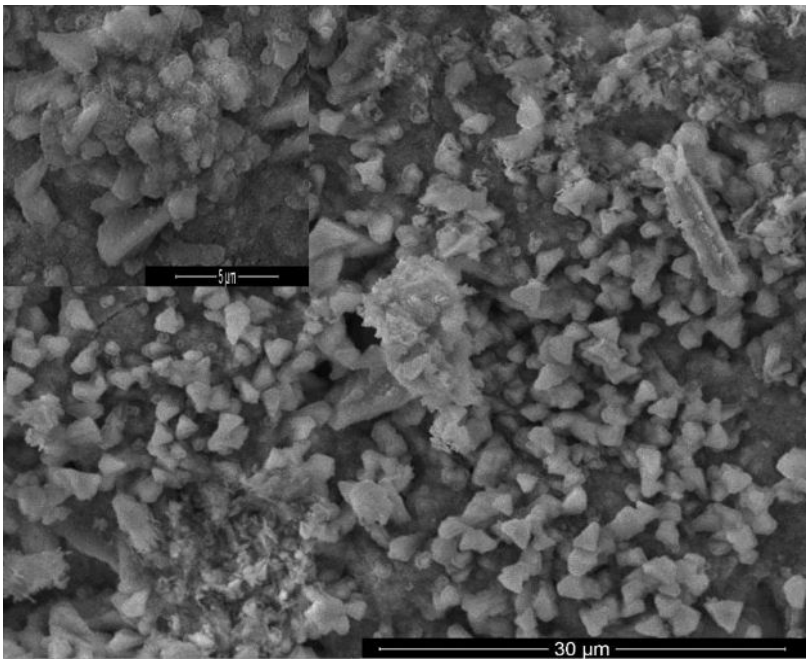

Fig. 4.42 SEM image of the surface of COMP-4 showing the proliferation and spreading of SCC-25 cells after 10 days of culture on COMP-4 (image at same magnification and scale bar represent 30µm (inset)

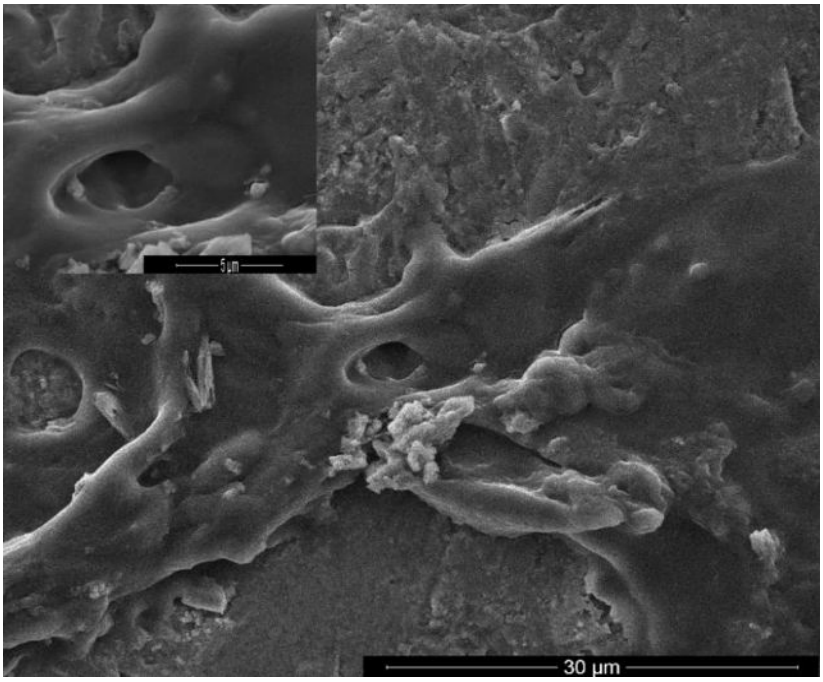

Fig. 4.43 SEM image of the surface of commercial dentine showing the proliferation and spreading of SCC-25 cells after 10 days of culture on dentine (image at same magnification and scale bar represent 30µm (inset)

4.3.9 Summary of the results

Mechanochemically derived leucite and kalsilte based bioactive glass ceramic composites have been prepared successfully for possible dental restorations. All the compositions show similar thermal and mechanical behavior to that of the commercial product. In the present study, the optimum bond has been achieved between the composite and substrate interface layer. The developed leucite and kalsilite bioactive glass ceramic composites applied as a veneer on the surface of commercial dental ceramic substrate generating bioactive coating. The leucite and kalsilite glass–ceramic composites are cytocompatible with negligible effect on cellular proliferation and direct cytotoxicity.

4.4 Effect of Al_2O_3 on leucite based bioactive glass ceramic composite for dental veneering

4.4.1 Phase analysis

Fig. 4.44 exhibits the XRD patterns of the composites before heat treatment. In the composites, leucite has been found to be a major crystalline phase along with alumina phase. The diffraction peaks matched to the JCPDS Card No. 87-1707 and 81-1667. It is seen that the intensity of the peak corresponding to Al_2O_3 phase increases with increasing the alumina content in the matrix. Fig. 4.45 shows the XRD patterns of the composite samples after heat treatment. The diffraction peaks matched to JCPDS Card No. 74-0387 and 81-1667.

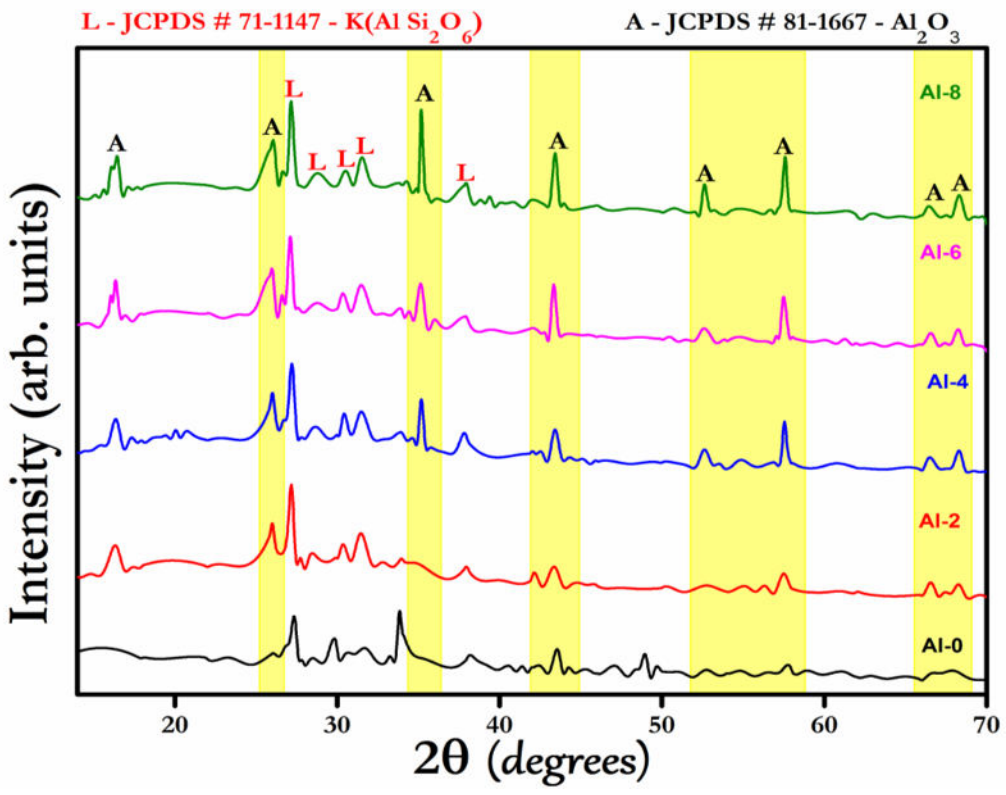

Fig. 4.44 XRD pattern of the composites containing different wt. % of alumina before firing

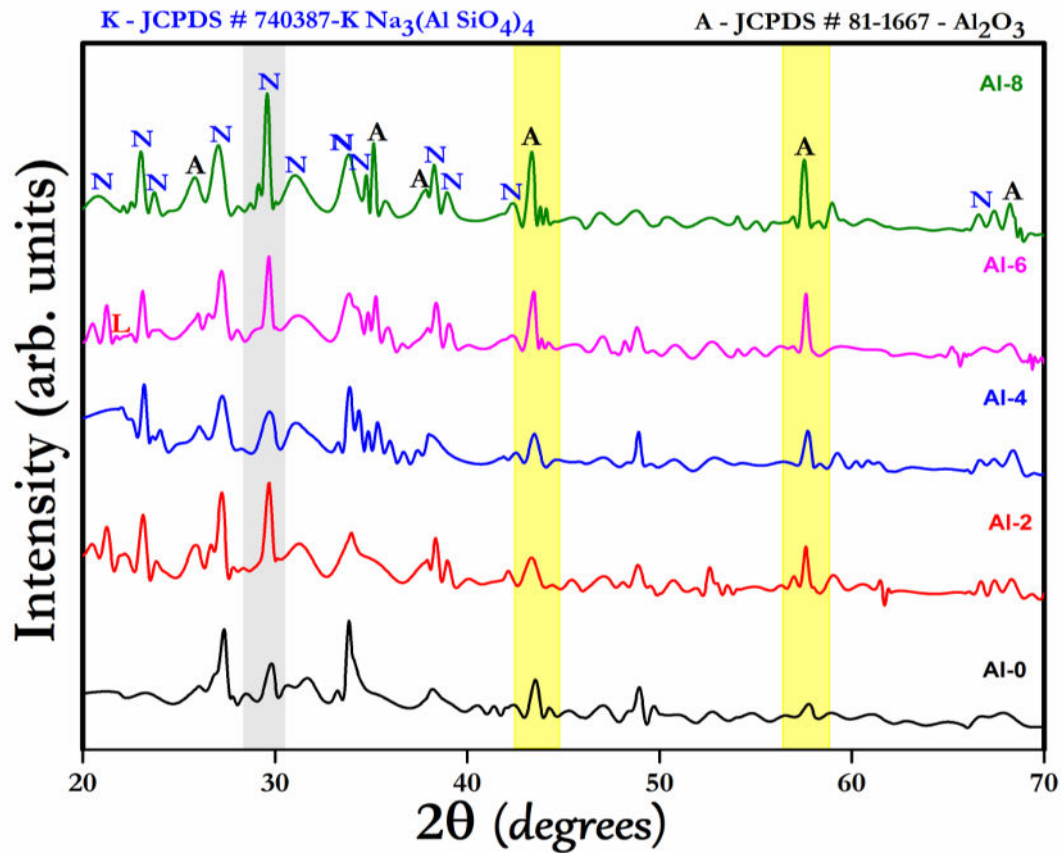

Fig. 4.45 XRD pattern of the composites containing different wt. % of alumina after heat treatment at 960 °C.

It is seen from Fig.4.45 that a major crystalline phase nepheline has formed after firing (at 950 °C) along with some alumina crystalline phase subsequently decreasing the amorphous phase. A second phase nepheline is formed due to the reaction of alumina with the free ions (K^+, Na^+ and Si^{4+}) present in the matrix during heat treatment. Nepheline has the high coefficient of thermal expansion and good mechanical strength which may further increase the mechanical properties of the prepared composites [Hamzawy E.M.A. and El-Meliegy E.A.M. 2008].

4.4.2 Microstructure

Figs. 4.46-4.48 show the surface morphology of Al-0%, Al-4% and Al-8% composites. It is seen that glassy surface reduces slightly with increasing the content of fine alumina in the composites. It is due to the presence of crystalline alumina particles which are distributed homogeneously in the glassy matrix. Micrographs show a very dense morphology with no visible micro-crack on the surface. SEM micrographs along with the EDX spectra of the compositions, Al-0% and Al-8% are shown in Figs. 4.49-4.50. EDX spectra confirm the presence of all the constituent elements (Na, K, Ca, Si, Al, O) in an expected concentration.

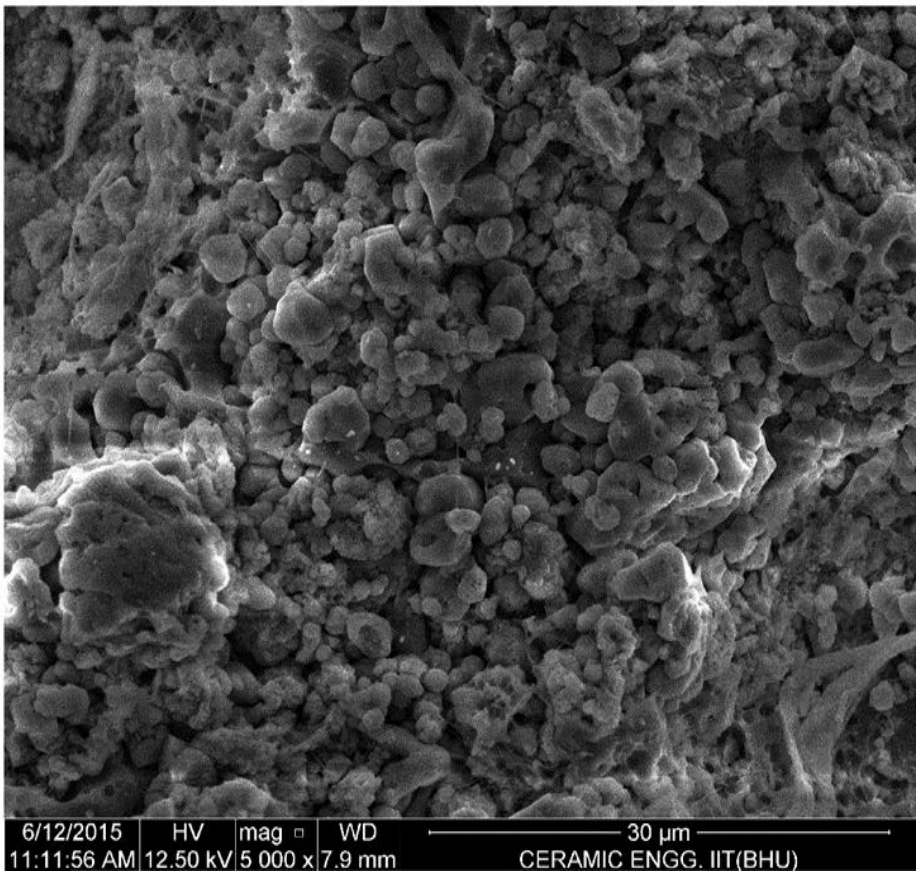

Fig. 4.46 SEM morphology of the composite Al-0 after heat treatment

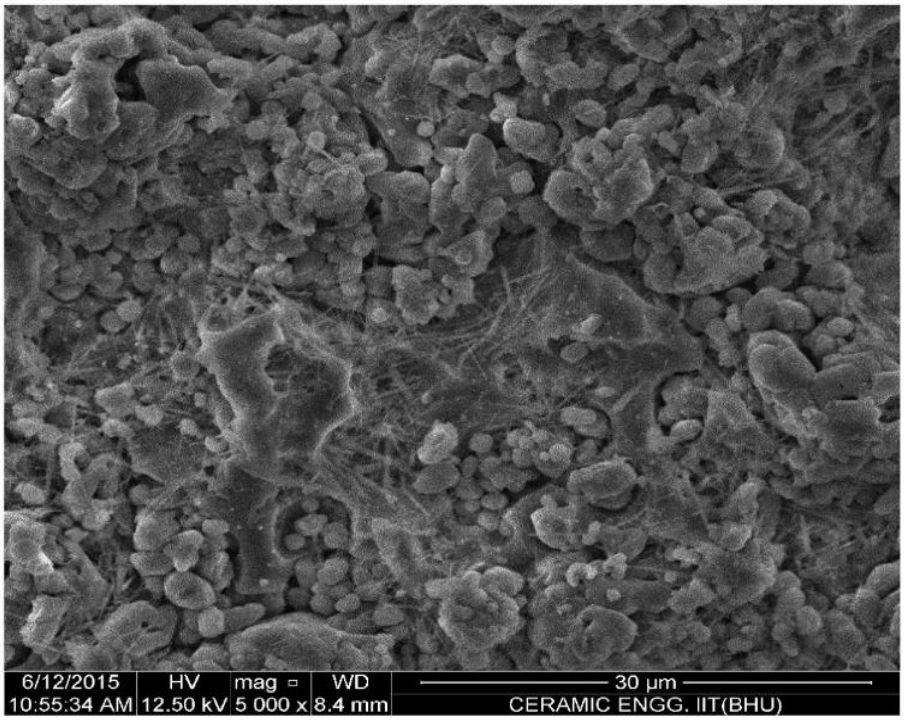

Fig. 4.47 SEM morphology of the composite Al-4 after heat treatment

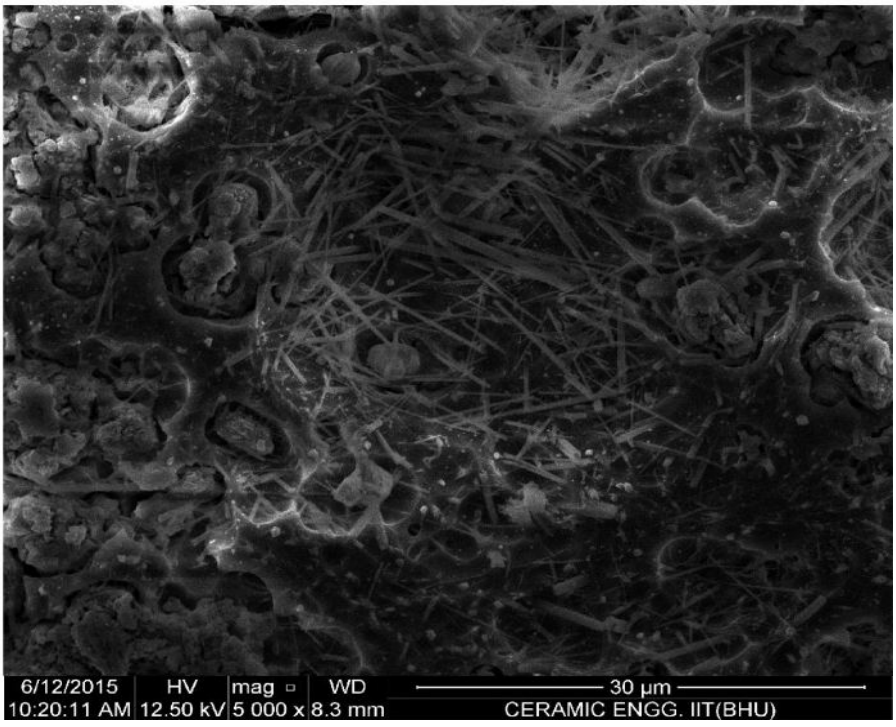

Fig. 4.48 SEM morphology of the composite Al-8 after heat treatment

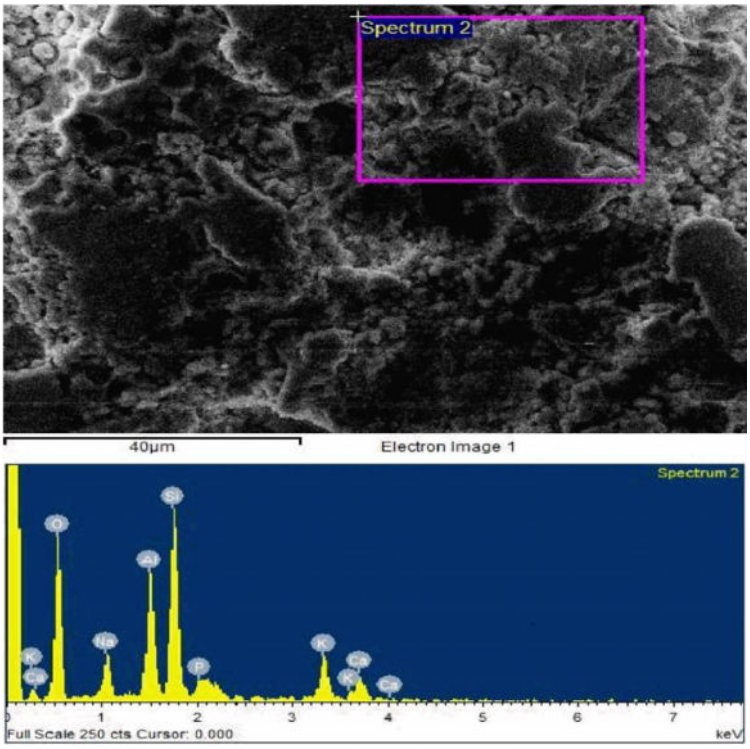

Fig.4.49 SEM and EDS spectrum of the composition Al-0

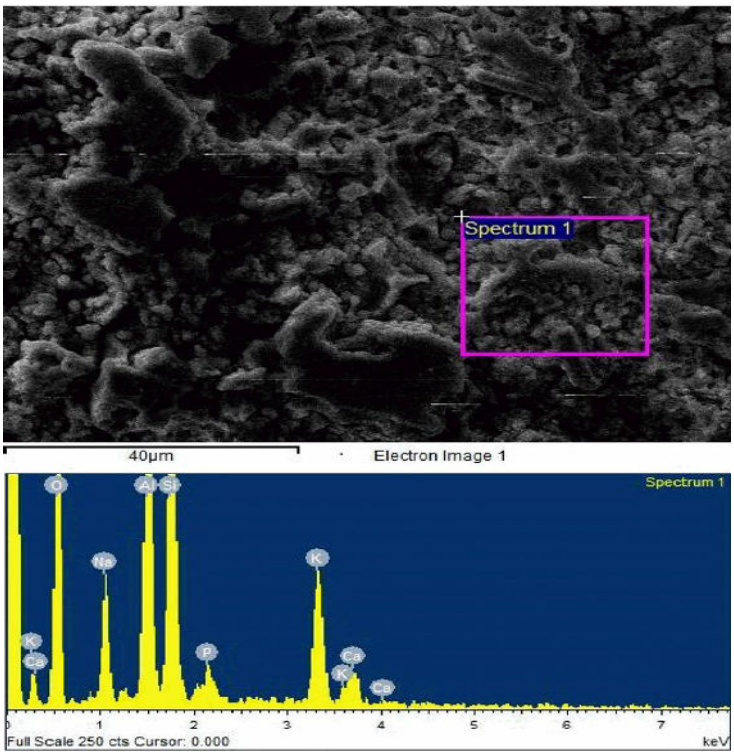

Fig. 4.50 SEM and EDS spectrum of the composition Al-8

4.4.3 Coefficient of thermal expansion (CTE)

Fig. 4.51 shows the CTE curves of the composites along with the commercial dentine (VITA VMK 2M2). It has been observed that the compositions, Al-0, Al-4, Al-8 and VITA dentine have CTE values 14.8×10^{-6}/°C, 15.0×10^{-6}/°C, 17.8×10^{-6}/°C and 14.5×10^{-6}/°C respectively. CTE of the composites, Al-0 and Al-4 is very close to that of commercial dentin. It is seen from Fig. 4.51 that thermal expansion of the composition Al-8 increases linearly i.e. there is no glass transition. It is due to the high content of alumina present in the matrix. It is found that the addition of fine alumina to the composites increases the CTE of the final mixture.

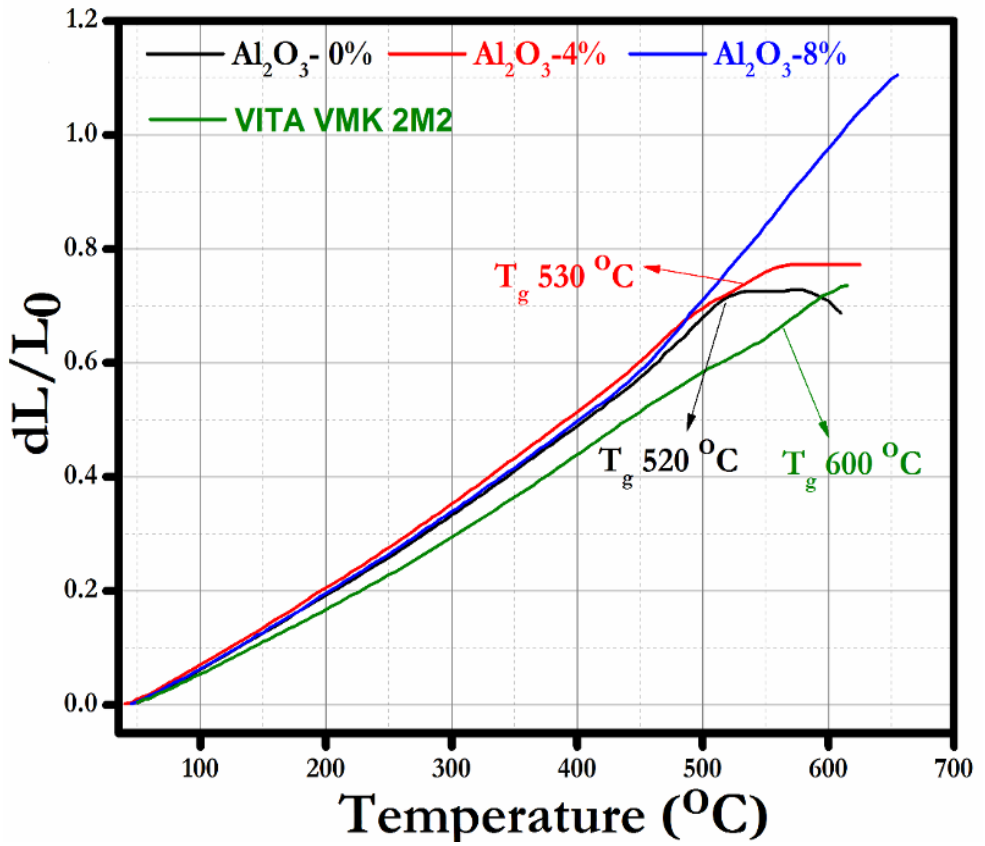

Fig. 4.51 CTE curves of the composites along with commercial dentine (VITA VMK 2M2)

This is due to the presence of nepheline crystalline phase (as seen from XRD patterns in Fig.4.45) which has the high CTE in the range 12.1-16.6×10^{-6}/K [Nan-Chung W. and Min-Hsiung H. 1994]. Khater et al. have also been reported that the formation of nepheline in the glass-ceramic increases the CTE of the matrix [Khater G.A. *et al.* 2013]. These prepared composite materials are, therefore, suitable for PFM as its CTE values are close to that of nickel–chrome alloy (13.9×10^{-6} /°C).

4.4.4 Bulk density (BD) and apparent porosity (AP)

Fig. 4.52 shows the BD and AP of the bioactive glass ceramic composites containing different wt. % of alumina. It is seen from Fig. 4.52 that BD increases (from 1.93 to 2.26 gm/cc) with increasing the alumina content followed by a continuous decrease in the AP.

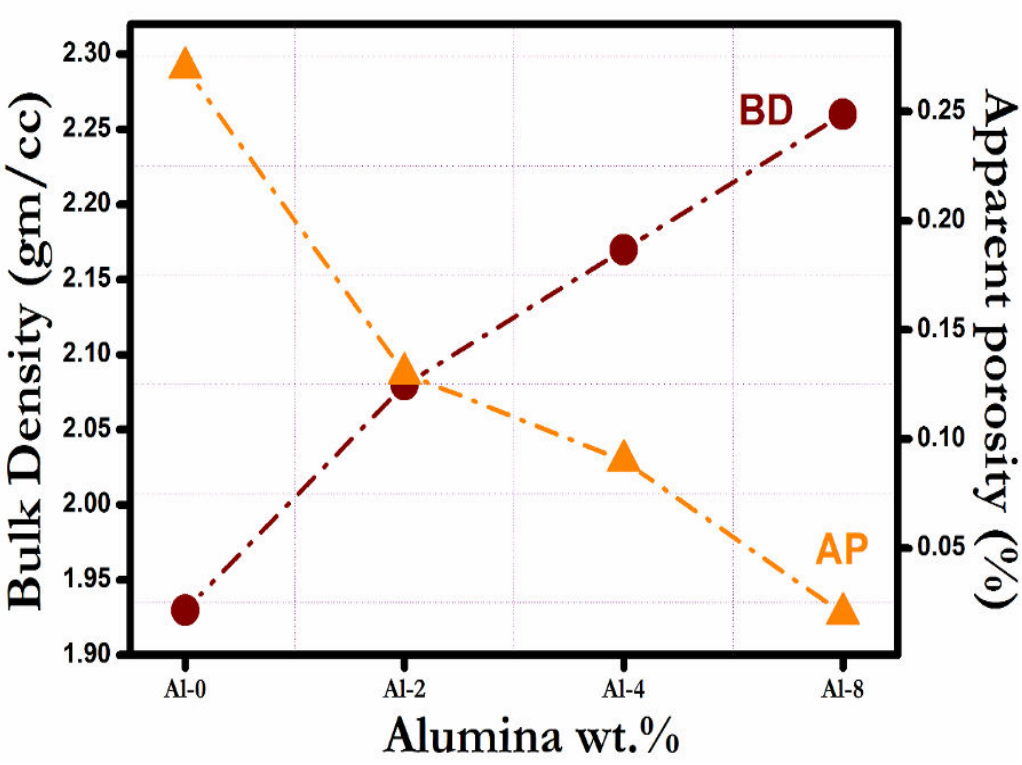

Fig. 4.52 BD and AP of the bioactive glass ceramic composites with different wt. % of alumina

Micro fine alumina particles homogeneously dispersed throughout the glassy matrix, improves the packing density of the composites consequently reduces the apparent porosity.

4.4.5 Flexural strength

Fig. 4.53 shows the flexural strength of the composite and the commercial dentine VITA VMK 2M2. Flexural strength increases with increasing the fine alumina in the matrix. Homogeneous dispersion of fine alumina particles within the glassy matrix leads to enhance the mechanical strength. This is because a crack cannot pass easily through the crystalline alumina particles whereas, in the case of a glassy matrix, it passes easily and hence decreases the mechanical strength.

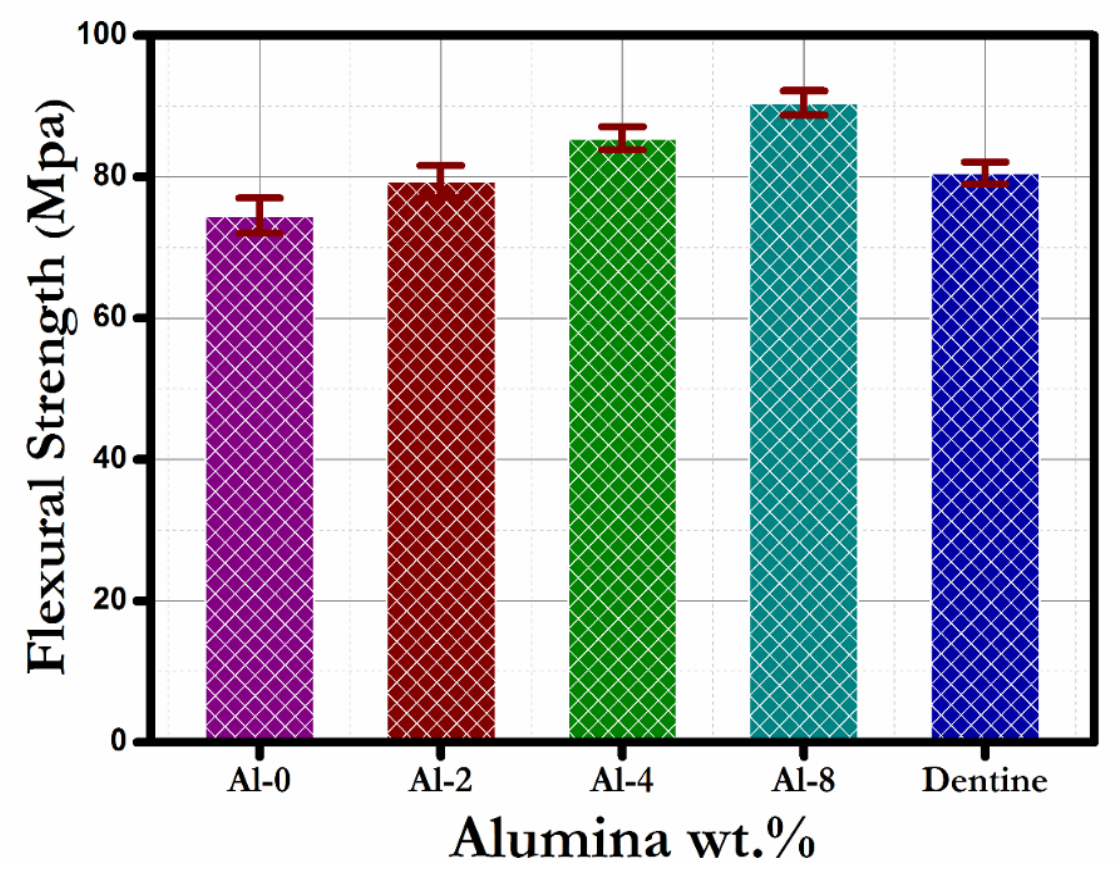

Fig. 4.53 Flexural strength of composites and commercial dentine

This technique has also been used in the dentistry for the development of aluminous porcelains [McCabe F.J. 2008]. Consequently, the synthesized composites show the superior sinterability, low porosity and high flexural strength. The strength of all the alumina added composites is nearly similar to that of the commercial dentine. One of the reasons for enhancement in the flexural strength of the alumina added composites is the formation of crystalline nepheline phase. It has also been reported in the literature that nepheline increases the mechanical strength of the glass-ceramics [Hamzawy E.M.A. and El-Meliegy E.A.M. 2008]. It is, therefore, concluded that fine alumina particles act as a 'crack stoppers' preventing the propagation of a crack throughout the body of the porcelain.

4.4.6 Culture of SCC-25 cells on glass–ceramic composites

Figs. 4.54 (a)-(d) show the surface morphology of the alumina added leucite glass–ceramic composites. SEM morphology reveals the proliferation of SCC-25 cells after 10 days of culture and it covers the whole surface of the sample. The images also show that the cells adhered to all the composites with a flattened and lengthened morphology. Higher numbers of cells are attached on the surface of composites Al-2 and Al-4. This is consistent with our results as observed concerning to growth inhibition and cytotoxicity [Fig.4.54 (b) & (c)]. These results also suggest that the prepared composite material allows the efficient growth of the cells over its surface (Fig. 4.54).

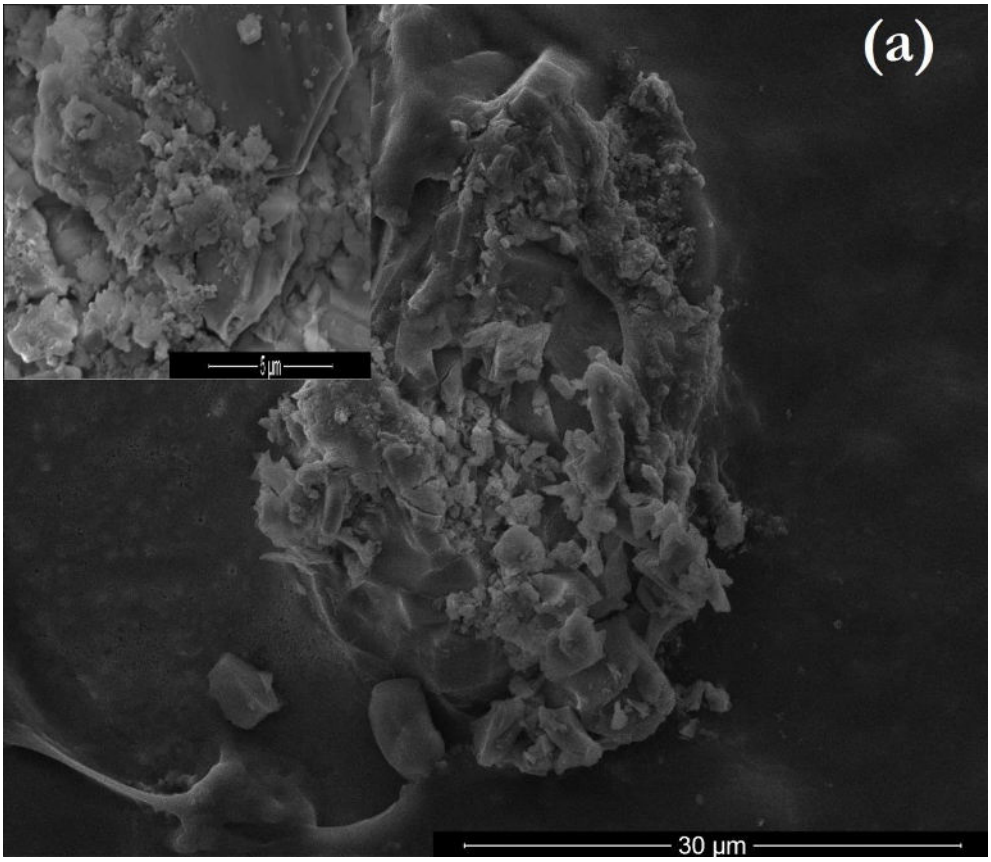

Fig. 4.54 (a) Surface morphology of the sample Al-0 showing the proliferation and spreading of SCC-25 cells after 10 days of culture

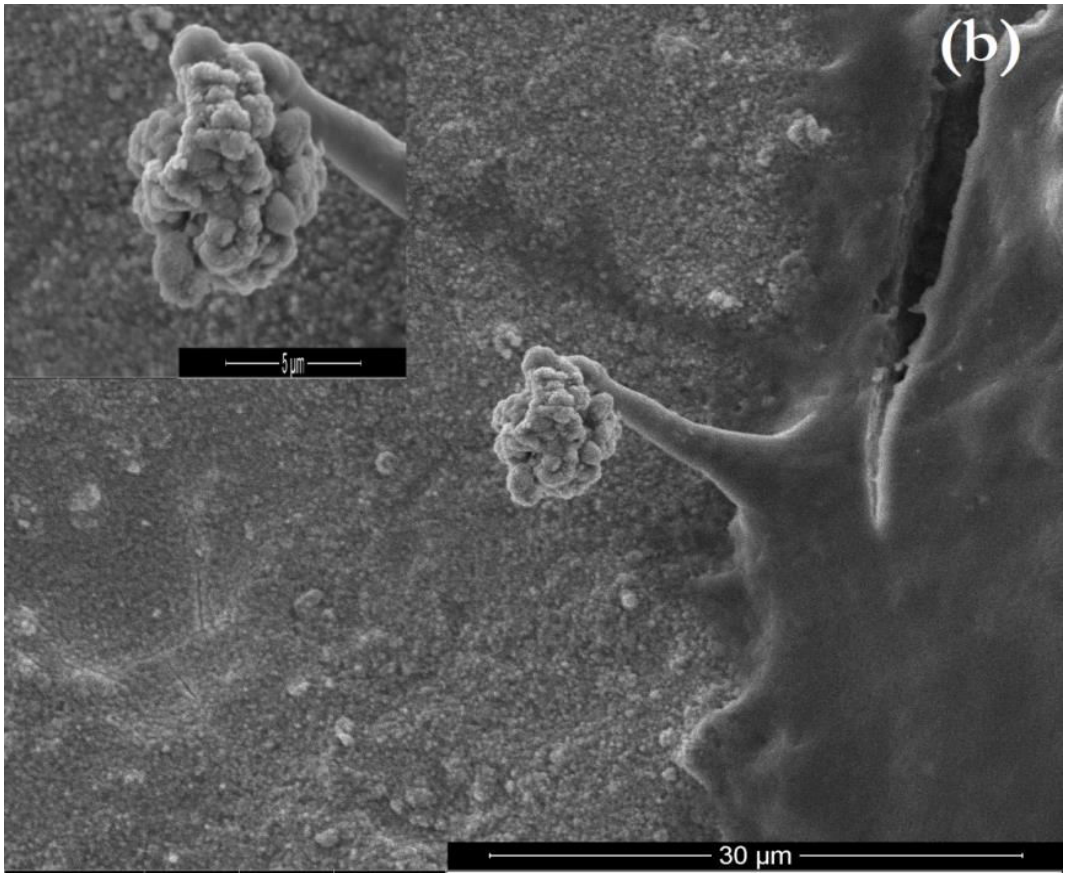

Fig. 4.54 (b) Surface morphology of the sample Al-2 showing the proliferation and spreading of SCC-25 cells after 10 days of culture

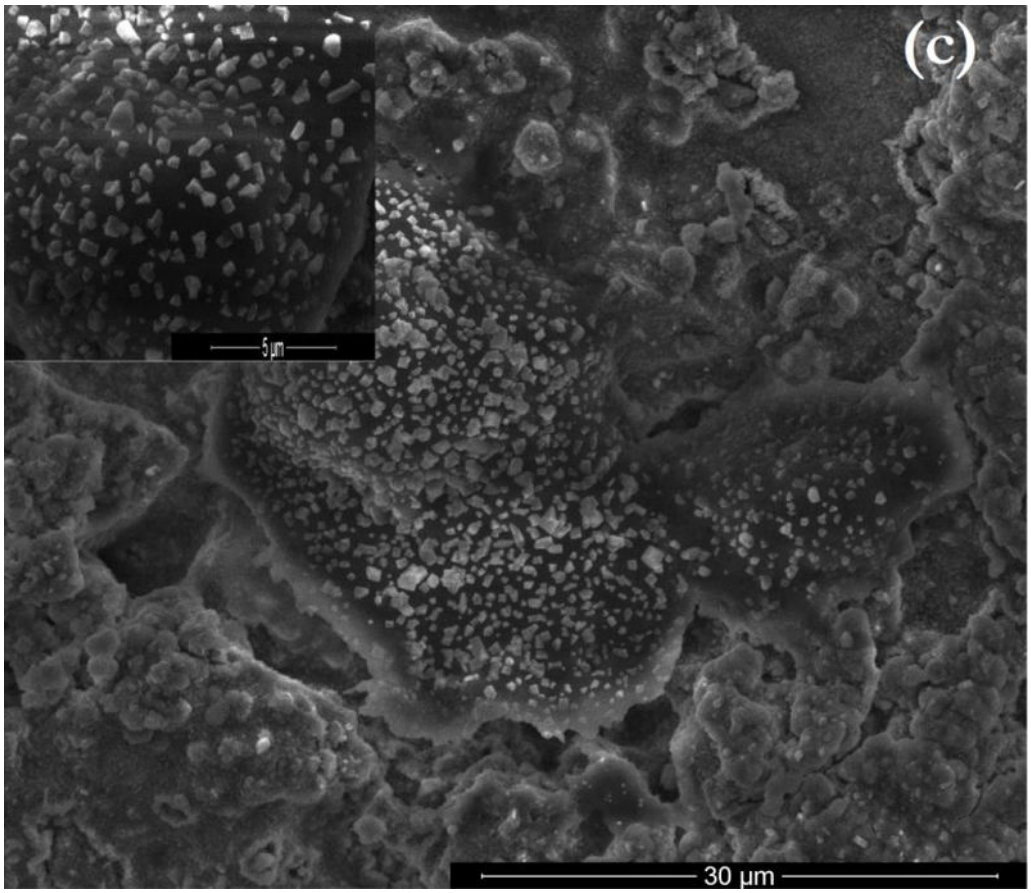

Fig. 4.54 (c) Surface morphology of the sample Al-4 showing the proliferation and spreading of SCC-25 cells after 10 days of culture

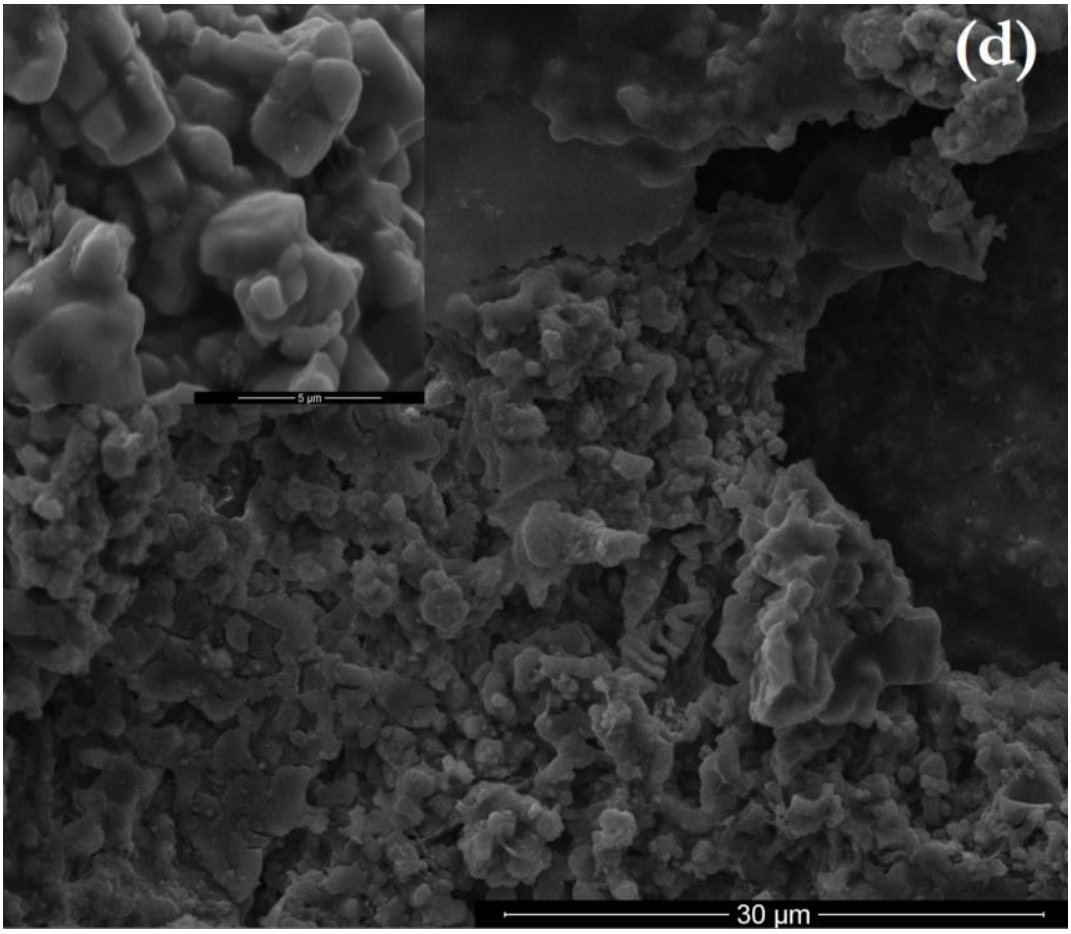

Fig. 4.54 (d) Surface morphology of the sample Al-8 showing the proliferation and spreading of SCC-25 cells after 10 days of culture

4.4.7 Summary of the results

This study has shown the successful investigation of alumina added leucite glass ceramic composites for possible applications in the dental restorations. The addition of alumina to the glass ceramic composites results in the formation of nepheline crystalline phase. This leads to enhance the CTE and flexural strength of the samples. Alumina added leucite glass ceramic composites show high flexural strength (80-90 MPa) than that of the leucite based glass ceramic composites (74-78 MPa) and the commercial dentine (79 MPa). A uniform attachment of SSC-25 cells after 10 days of culture on the surface of the composites has been observed. It confirms that the addition of alumina to the leucite glass ceramic composite is a successful approach to improving its mechanical and biological properties.